

POLITECNICO DI TORINO

Collegio di Ingegneria Chimica e dei Materiali

**Corso di Laurea Magistrale
in Ingegneria Chimica e dei Processi Sostenibili**

Tesi di Laurea Magistrale

**Chain-growth versus step-growth
polymerization in an aerosol photo-induced
process**



Relatore

prof. Marco Sangermano

Candidato

Diego Longo

Dicembre 2019

Contents

Abstract	i
0.1 Obiettivo della tesi	i
0.2 Introduzione	i
0.3 Risultati	iii
0.3.1 Polimerizzazione a step: meccanismo radicalico tiolo-ene	iii
0.3.2 Polimerizzazione a catena: meccanismo radicalico acrilico	ix
0.4 Conclusioni	xiii
1 Introduction	1
1.1 Overview of microscaled and nanoscaled systems	1
1.2 Production of micro and nanoparticles	2
1.3 Mechanisms of polymerization	4
1.3.1 Thiol-ene radicalic step-growth polymerization	4
1.3.2 Acrylic radicalic chain-growth polymerization	5
1.4 The aerosol photopolymerization technique in the scientific literature	7
1.5 Aim of the work	8
2 Experimental section	9
2.1 Materials	9
2.2 Equipment and instrumentation	10
2.3 Analysis Techniques	14
3 Results and discussion: Step polymerization	15
3.1 Variation of Ene-monomer	15
3.2 Variation of Thiol monomer	18
3.3 Effect of different co-solvents	20
3.4 Effect of the amount of co-solvent	24
3.5 Effect of the variation of monomers to solvents ratio	26
3.6 Usage of different atomizers	27
3.7 Usage of the three models of photoreactor	29
3.8 The addition of a soft-maker: Glycerol	31
3.9 Incorporation of silver nanoparticles	36
4 Results and discussion: Chain polymerization	39
4.1 Morphology of acrylic polymer particles	39
4.2 Effect of porogens: Hexadecane	44
4.3 Effect of porogens: Isooctanol	45
4.4 Effect of porogens: 2-Octanone	49
4.5 Incorporation of silver nanoparticles	50
Conclusions	53

List of Figures	58
List of Tables	59
Acronyms	61
Bibliography	63
Acknowledgements	65

Abstract

Il lavoro, qui di seguito illustrato, è stato condotto presso i laboratori del MAB (Molekulare Aufarbeitung von Bioprodukten) del Karlsruhe Institute of Technology (KIT) in Karlsruhe, Germania.

0.1 Obiettivo della tesi

Nella trattazione verranno descritti due differenti meccanismi di polimerizzazione. L'attenzione è focalizzata sulle principali differenze riscontrate tra polimerizzazione tiolo-ene (a step) e polimerizzazione acrilica (a catena) in un processo di fotopolimerizzazione in aerosol. Tali differenze sono incentrate sulla variazione e ottimizzazione delle apparecchiature utilizzate per la produzione di micro e nano-particelle polimeriche. Per di più, è stata analizzata la composizione della soluzione spray di partenza e come essa sia in grado di modificare la morfologia e la dimensione delle particelle ottenute.

0.2 Introduzione

Oggigiorno, l'impiego di micro-particelle polimeriche è ampiamente diffuso in molte applicazioni scientifiche come ricerca medica, analisi immunologiche, modellizzazione di fenomeni fisici e realizzazione di supporti catalitici e cromatografici (Esen and Schweiger, 1996). Per micro-particella è intesa una particella sferica con diametro compreso nel range 1-1000 μm (Campos et al., 2013).

Per quanto riguarda le nano-particelle, vari studi sono stati condotti sull'impiego di essere nel trasporto di principi attivi e molecole biologiche (Cruz et al., 2006). In particolare, la loro dimensione subcellulare favorisce l'assorbimento all'interno di sistemi microscopici e la loro capacità di stabilizzare le sostanze trasportate in combinazione con la loro costituzione biocompatibile le rende protagoniste nel settore farmaceutico biomolecolare (Furtado et Al., 2001 a,b; Guinebretière et al., 2002). Nano-particelle sono definite le particelle sferiche avente diametro generalmente compreso fra i 100 e i 500 nm (Liu, 2006).

I metodi di preparazione di micro- e nano-particelle sono molteplici. Nel corso degli anni, sono state sviluppate molte tecniche che sfruttano una polimerizzazione in fase liquida, ma l'alternativa studiata negli ultimi anni riguarda la tecnica della fotopolimerizzazione in aerosol. La nebulizzazione di gocce liquide in una matrice gassosa in un processo attivato fotochimicamente permette di avere molti vantaggi rispetto ai processi concorrenti, per la formazione di micro-strutture. Fra questi è possibile notare un'elevata purezza del prodotto ottenuto, la possibilità di condurre prove a temperature non elevate (Biskos et al., 2008), riduzione della produzione di sostanze di scarto, possibilità di limitare il fenomeno della polimerizzazione in un micro-sistema corrispondente alla bolla nebulizzata e la possibilità di gestire più parametri del processo contemporaneamente (diametro delle particelle prodotte, tempo di polimerizzazione, etc.).

L'atomizzazione della soluzione liquida può avvenire per via pneumatica, ultrasonica o elettro-idrodinamica. Nella seguente tesi è stato utilizzato il principio pneumatico, che, dopo aver creato le bolle, grazie ad un flusso di azoto puro le trasporta all'interno del fotoreattore dove avviene la polimerizzazione.

Sono stati confrontati i meccanismi di polimerizzazione a step attraverso delle reazioni tiolo-ene e quello di polimerizzazione a catena attraverso reazioni che coinvolgono esclusivamente monomeri acrilici.



Figura 1: L'intera strumentazione utilizzata con atomizzatore, reattore e filtro per la raccolta del prodotto.

La soluzione, preparata e contenuta all'interno di un recipiente, è nebulizzata dall'atomizzatore per mezzo di un ugello a due componenti, che sfrutta la forza pneumatica fornita dalla corrente di azoto puro alimentata. La dimensione delle gocce nebulizzate ha raggiunto al massimo la dimensione di 1 μm . Un abbattitore interno all'apparecchiatura garantisce la corretta separazione dimensionale delle gocce. Sono stati comparati due differenti modelli di atomizzatori che sfruttano diverse tecniche di separazione dimensionale delle gocce. Allo stesso tempo sono stati confrontati anche tre modelli di reattori differenti che simulavano un cambiamento di geometria, materiale di composizione e tempo di permanenza disponibile alla polimerizzazione. Tutti i modelli di reattore utilizzati sono stati irradiati dalla stessa batteria di 6 lampade UV che hanno emesso una radiazione policromatica dalla lunghezza d'onda compresa nel range 270-360 nm, con un picco di emissione a 312 nm. La maggior parte degli esperimenti è stata condotta alla pressione di 1 bar; solo per il reattore a 2-tubi la pressione è stata modificata a 0,5 bar e 0,7 bar per garantire una raccolta minima del polimero prodotto e permetterne l'analisi.

Per il meccanismo tiolo-ene il sistema di raccolta consisteva in un tubo in plastica a spirale, dove il polimero aderiva alla sua superficie interna e veniva successivamente raccolto con l'aiuto di un solvente; per i polimeri acrilici, è stata utilizzata una membrana PTFE avente pori con un diametro medio di 100 nm. Essa veniva cambiata ogni 30 minuti per evitare l'otturazione e la creazione di una sovrappressione all'interno del sistema. La durata di ogni esperimento è stata di almeno 1 ora per le polimerizzazioni acriliche e di circa 2 ore per il meccanismo tiolo-ene.

Successivamente, i polimeri sono stati raccolti in delle provette contenenti acetone e agitati per almeno 24 h prima di essere analizzati. Gli esperimenti riguardanti l'incorporazione di nanoparticelle di argento hanno avuto un'analogia procedura di esecuzione fuorché per il loro tempo di preparazione: le soluzioni contenenti le miscele di argento sono state agitate per almeno 24 h prima di essere nebulizzate.

La caratterizzazione delle particelle è avvenuta per mezzo di immagini al FE-SEM (Leo Gemini 1530, Carl Zeiss, Oberkochen, Germany), una tecnica che ha permesso di individuare morfologia e dimensione delle stesse. Immagini al TEM sono state utilizzate invece per determinare l'esito della produzione di particelle *in situ*.

0.3 Risultati

Basandosi sui risultati ottenuti da inerenti studi condotti negli anni precedenti, il lavoro è partito con la riproduzione di alcuni esperimenti al fine di verificarne l'esito. In entrambe le parti in cui è suddivisa la trattazione si è cercato di comprendere quali sono le cause della variazione della morfologia delle particelle prodotte. Perciò, in primo luogo, verranno trattati gli aspetti della polimerizzazione radicalica tiolo-ene, mentre nella seconda parte verrà trattato ciò che concerne la polimerizzazione acrilica radicalica.

0.3.1 Polimerizzazione a step: meccanismo radicalico tiolo-ene

Il primo passo è stato individuare quali fossero i binomi di monomeri più adatti alla realizzazione di micro-particelle tramite fotopolimerizzazione in aerosol. Diverse serie di esperimenti sono stati condotti prima utilizzando il solo Trimethylolpropane Tri(3-mercaptopropionate) (TMPMP) e variando il monomero contenente il doppio legame carbonio-carbonio. Dopodichè anche il mercaptano è stato variato mantenendo nella composizione della soluzione spray il monomero acrilico Trimethylolpropane triacrylate (TMPTA). Micro-capsule sono state ottenute con il binomio TMPMP-TMPTA in una soluzione omogenea (Figura 2) contenente esadecano (HD), 2-ottanolo e isoottanolo come solventi ed etanolo come co-solvente con un rapporto monomero-solvente di 33:67.

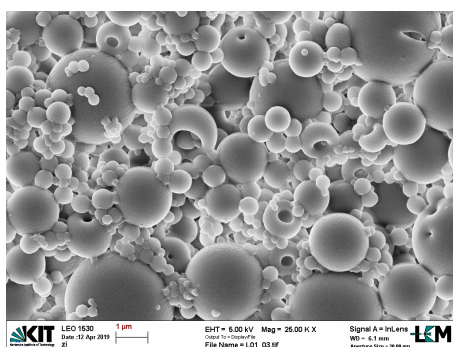


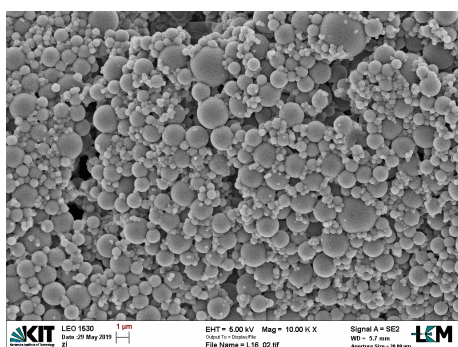
Figura 2: Immagine al FE-SEM di micro-capsule ottenute con TMPMP-TMPTA.

Le altre combinazioni hanno fornito morfologie poco interessanti da un punto di vista applicativo. Alcuni polimeri formati, sono caratterizzati da una matrice appiccicosa con particelle polimeriche non definite, mentre altre combinazioni hanno causato problemi alle apparecchiature durante il corso degli esperimenti, poichè la soluzione di partenza si presentava torbida ed eterogenea.

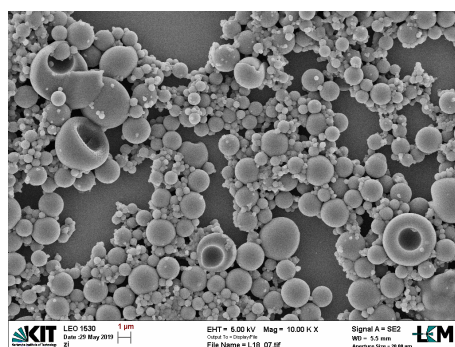
Data la differente velocità di formazione dei radicali da parte dei due monomeri (più bassa nel caso dei mercaptani), la struttura potrebbe dipendere dallo step limitante della reazione. Perciò il numero di gruppi funzionali coinvolti all'interno della reazione ha un ruolo fondamentale

poiché possono accelerare o rallentare il meccanismo di polimerizzazione. Monomeri con 3 o 4 gruppi funzionali hanno la capacità creare strutture polimeriche ramificate, più adatte alla formazione di micro-capsule.

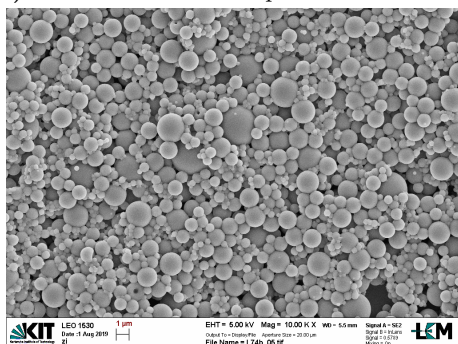
Una volta individuate le combinazioni più interessanti dal punto di vista morfologico delle particelle, sono stati analizzati i diversi effetti dei solventi che diluiscono i reagenti nella soluzione spray. Il ruolo del co-solvente si è dimostrato determinante per la formazione di micro-capsule e per la stabilizzazione della soluzione durante tutta la durata dell'esperimento. Diverse serie di prove sono state effettuate mantenendo invariata la quantità di solventi nella soluzione e variando la tipologia del co-solvente fra etanolo, 1-propanolo e acetone. Sebbene alcune prove non abbiano prodotto particelle di forma regolare e ben distaccate fra loro, si è comunque evinta l'importanza della scelta del co-solvente impiegato.



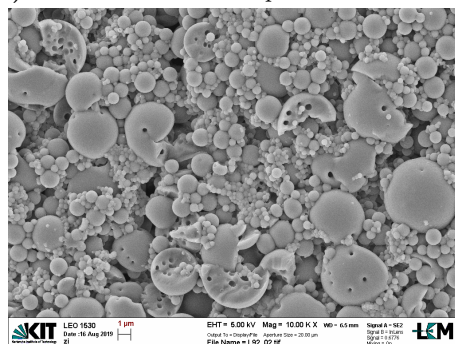
(a) TMPMP-TMPTA in presenza di etanolo.



(c) TMPMP-TMPTA in presenza di acetone.



(b) TMPMP-TMPTA in presenza di 1-propanolo.



(d) TMPMP-TMPTA in assenza di co-solvente.

Figura 3: Immagini al FE-SEM di particelle di TMPMP-TMPTA ottenute con i diversi co-solventi.

Una volta avvenuta la polimerizzazione, il polimero formatosi riveste lo strato esterno della goccia, mentre il nucleo è composto prevalentemente dai solventi liquidi. Una maggiore volatilità del co-solvente permette di occupare grandi frazioni di volume all'interno della goccia nebulizzata che si traduce in un maggiore grado di vuoto dopo l'evaporazione. Il collasso del guscio polimerico è stato osservato nelle particelle di maggiore dimensione che ha portato alla formazione di micro-capsule più o meno accentuata. Naturalmente, se il polimero è abbastanza rigido da sostenere la struttura a guscio, il collasso dello stesso non avviene. L'acetone si è mostrato più affine alla produzione di capsule con la combinazione TMPMP-TMPTA, in quanto solubilizza svariati reagenti impiegati e si presenta come il più volatile fra i 3 co-solventi. Tuttavia, come precedentemente mostrato in Figura 2 anche con l'etanolo è stato possibile produrre micro-capsule.

Sebbene la scelta del co-solvente sia importante per determinare la morfologia, la quantità di esso aggiunta alla soluzione spray non ha dimostrato alcuna influenza sulla forma ottenuta. Essa sembra però influire sulla dimensione delle particelle. Diversi esperimenti sono stati effettuati raddoppiando, triplicando la quantità aggiunta o addirittura in assenza di co-solvente (solo

per la combinazione TMPMP-TMPTA che si è mostrata omogenea in qualunque condizione esaminata), ma nessuna regola generale è stata osservata. In assenza di co-solvente, infatti sia nano-particelle che micro-particelle sono state prodotte e le più grandi presentano numerosi pori alla superficie (Figura 3d).

La quantità di co-solvente aggiunta modifica anche il rapporto monomero-solvente della soluzione spray. Per evidenziare l'influenza di questo parametro, sono stati condotti due esperimenti in cui varia il rapporto monomero-solvente. Con la medesima combinazione di monomeri sono stati confrontati un rapporto di 50:50, come quello in Figura 3d e un rapporto 29:71, con il quale si sono prodotte particelle dal diametro decisamente ridotto, ma non ben definite come nel primo caso. La formazione di oligomeri a bassi valori di rapporto M/S è favorita per via della bassa percentuale di reagente contenuta all'interno di ogni singola goccia. Gli oligomeri sono i responsabili della formazione di ponti di collegamento fra le varie particelle, la cui forma sferica viene compromessa. La ridotta quantità di monomero in ogni goccia è anche responsabile della diminuzione del diametro medio particellare.

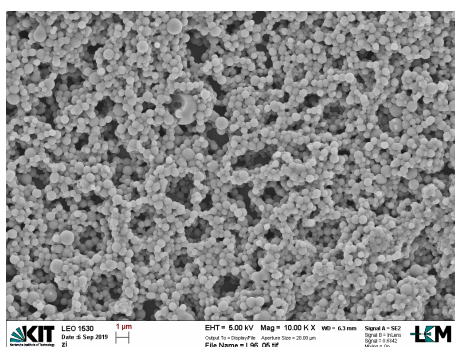


Figura 4: Immagine al FE-SEM di particelle TMPMP-TMPTA con rapporto M/S pari a 29:71.

Fra i due esperimenti effettuati è stato anche variato il rapporto fra la quantità di solventi. L'esadecano è un cattivo solvente e come tale ha il ruolo di accentuare la separazione di fase durante la polimerizzazione all'interno di ogni goccia che attraversa il reattore. La sua quantità è stata diminuita dal 54% dei solventi totali al 30% nell'esperimento in Figura 4 e di conseguenza la separazione di fase è stata ritardata. Il 2-ottanone è buon solvente e contribuisce a ritardare la gelificazione del polimero così come l'isottanolo: entrambi sono i responsabili della formazione di pori all'interno delle particelle. La diminuzione della quantità di esadecano, in percentuale, porta alla produzione di particelle meno definite e accentua i ruoli degli altri 2 solventi che contribuiscono a rendere più appiccicosa la matrice polimerica. Infine, la produzione di particelle polimeriche porose sembra essere favorita dalla dimensione delle particelle: maggiore è il diametro, più elevata sarà la probabilità di evaporazione dei solventi da punti differenti dall'interno della goccia. Un basso rapporto M/S senza aggiunta di solvente difficilmente porta alla formazione di pori.

Mantenendo costante la composizione della soluzione spray, è stato valutato anche l'effetto dei diversi modelli di apparecchiature utilizzate. Le performance degli atomizzatori sono state misurate nel reattore a doppio tubo, che ha modificato i risultati precedentemente commentati. L'utilizzo di due differenti modelli, alle stesse condizioni operative, ha portato alla formazione di particelle prevalentemente identiche sia in termine di morfologia che di dimensione. Pertanto, il meccanismo di funzionamento non ha condizionato l'esito degli esperimenti. Ciò che ha invece influito, è stata l'aggiunta del flusso di azoto puro alla corrente nebulizzata, che potrebbe aver favorito l'evaporazione delle sostanze più volatili dal bulk delle gocce. Infatti, sebbene il tempo di permanenza nel reattore sia stato notevolmente ridotto, numerose micro-capsule sono state prodotte con l'impiego di TMPMP-TMPTA in presenza di acetone (Sezione 3.6).

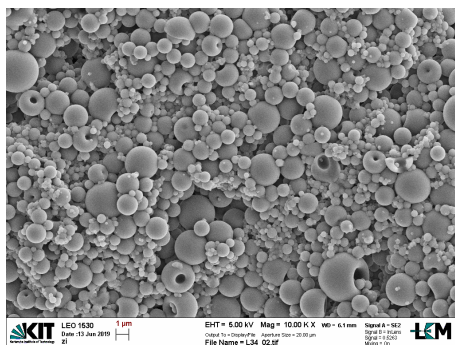
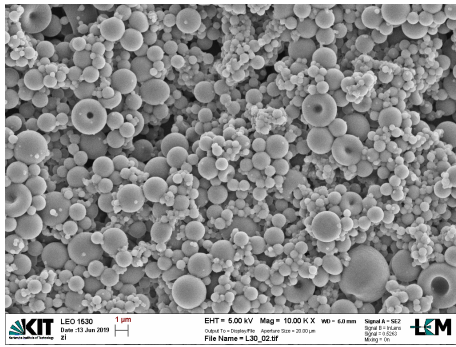


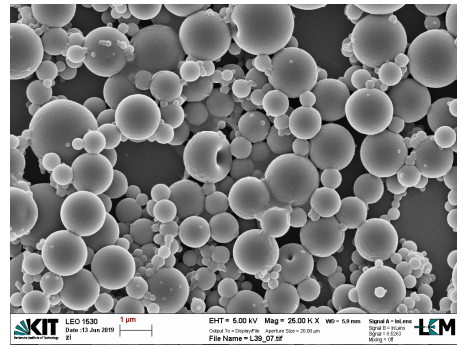
Figura 5: Immagine al FE-SEM di micro-capsule ottenute con TMPMP-TMPTA.

La scelta del modello di reattore ha influenzato la morfologia delle particelle ottenute. Il reattore a 2 tubi, di etilene propilene fluorurato, ha prodotto particelle sferiche piene per via del ridotto tempo di permanenza, pari a circa 11 secondi. Il reattore a 4 tubi dello stesso materiale, con un tempo di permanenza di circa 14 secondi, ha portato alla formazione di micro-capsule di forma irregolare e varie particelle cave di dimensione superiore al micrometro (Figura 6c). Il reattore a tubo di quarzo, invece, ha fornito micro-capsule ben definite (Figura 6a) con un tempo di permanenza di oltre 36 secondi.

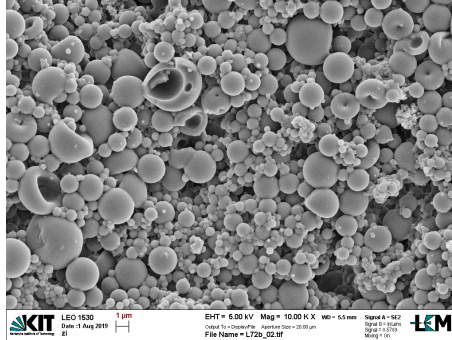
La quantità di fotoiniziatore attivato è strettamente legata al tempo di permanenza. Al diminuire di quest'ultimo, lo step di propagazione è favorito rispetto a quello di formazione del radicale e la reazione rallenta notevolmente. Lo step controllante ritarda la separazione di fase per via della minore quantità di polimero formatosi, con il risultato di una matrice polimerica più appiccicosa. Le caratteristiche strutturali potrebbero essere legate anche al cambiamento del materiale con diversa trasmittanza delle radiazioni. Tale rallentamento comporta il completamento degli step di propagazione e terminazione all'interno del tubo a spirale (dove il materiale viene prelevato), nonostante il materiale non sia più esposto alle radiazioni luminose. Anche la combinazione di monomeri PETMP-TMPTA (rapporto molare 1:1,33) ha confermato l'influenza del tempo di residenza sul meccanismo tiolo-ene, fornendo, però, micro-capsule solo nel reattore a tubo di quarzo.



(a) Micro-capsule di TMPMP-TMPTA.



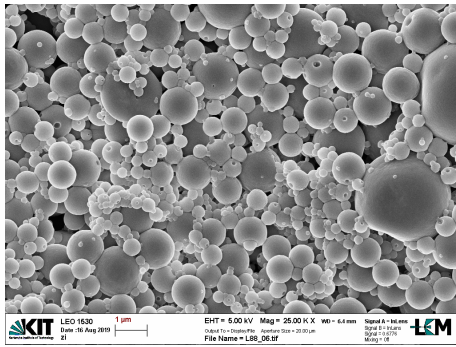
(b) Micro-capsule di PETMP-TMPTA.



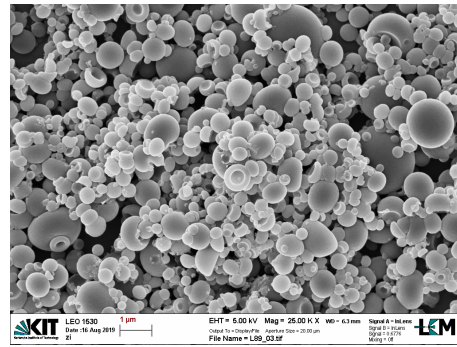
(c) Micro-capsule irregolari di TMPMP-TMPTA.

Figura 6: Immagini al FE-SEM di micro-capsule ottenute con meccanismo tiolo-ene.

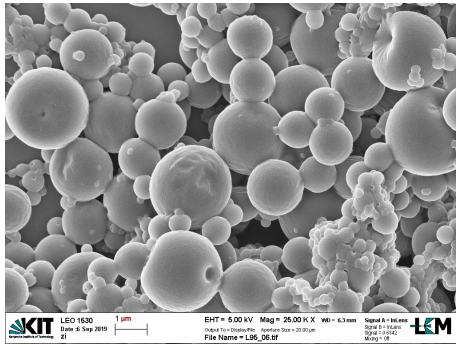
Per la produzione di nano-capsule e nano-caps, è stato aggiunto il glicerolo alle precedenti soluzioni spray. Pertanto, le combinazioni PETMP-TMPTA e TMPMP-TMPTA sono state testate nel reattore a 4 tubi di etilene propilene fluorurato. L'aggiunta di glicerolo alle soluzioni contenenti acetone ha causato molti problemi al processo (separazione di fase all'interno della soluzione spray, blocco dell'ugello), dal momento che l'acetone non solubilizza il poliolo. Infatti, oltre ai problemi al setup, non si sono visti netti cambiamenti dal punto di vista morfologico con entrambi i binomi. Alcune nano-capsule sono tuttavia osservabili in Figura 7a. L'impiego di etanolo invece si è rivelato risolutivo, in quanto più affine al glicerolo. La soluzione spray è rimasta stabile (anche se non limpida) per tutta la durata dell'esperimento e il suo effetto di "soft-maker" nella polimerizzazione è stato confermato anche per il meccanismo tiolo-ene. Diminuendo la rigidità dei polimeri è stato reso possibile il collasso delle particelle di dimensione minore al micron, producendo così una considerevole quantità di nano-caps con entrambe le combinazioni.



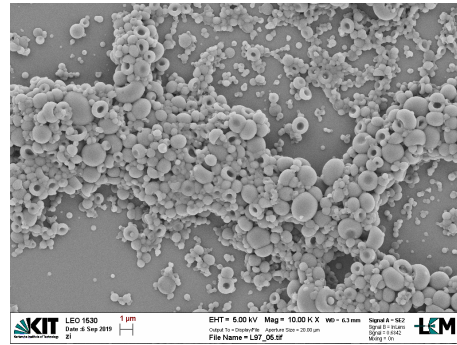
(a) PETMP-TMPTA con glicerolo in acetone.



(b) PETMP-TMPTA con glicerolo in etanolo.



(c) TMPMP-TMPTA con glicerolo in acetone.



(d) TMPMP-TMPTA con glicerolo in etanolo.

Figura 7: Immagini al FE-SEM di nano-capsule e nano-caps ottenute con meccanismo radicalico tiolenico.

Infine, è stata tentata la produzione *in situ* di particelle organiche-inorganiche ibride. L'obiettivo era quello di incorporare in micro-capsule e nano-caps, delle nano-particelle di argento. Vari tentativi sono stati effettuati con la combinazione TMPMP-TMPTA ottenendo però un esito negativo. La caratterizzazione delle particelle è avvenuta attraverso scansioni al TEM. Nonostante l'impiego di diverse forme di nano-particelle di argento (illustrate nella sezione 0.2), in ogni caso si è verificata la creazione di agglomerati del diametro di circa 2 μm al di fuori della matrice polimerica. Le possibili problematiche potrebbero essere legate all'interazione che l'argento mostra con i radicali tiolenici, durante lo step di propagazione e con il fotoiniziatore quando è scisso per via dei raggi UV incidenti. Infatti, tali interazioni hanno modificato anche la morfologia delle particelle osservate al FE-SEM. Le formulazioni, precedentemente menzionate per la formazione di capsule, hanno in questo caso prodotto una matrice polimerica confusa e irregolare.

0.3.2 Polimerizzazione a catena: meccanismo radicalico acrilico

L'approccio metodologico utilizzato è simile a quello effettuato per il meccanismo tiolo-ene. Il primo esperimento ha voluto mostrare i risultati di una polimerizzazione meramente acrilica, del solo monomero TMPTA con lo stesso rapporto M/S di 33:67 e stessa concentrazione di solventi e co-solventi utilizzati per l'esperimento in Figura 2, dove sono state ottenute delle micro-capsule. Il risultato, mostrato nella figura sottostante, riporta una struttura polimerica a mosaico con micro-particelle ad elevata area superficiale. La superficie è caratterizzata da domini polimerici della dimensione dell'ordine di decine di nanometri, anch'essi strutturati. Questa particolare struttura è stata quindi studiata ed in generale le morfologie ottenute da altri 4 monomeri acrilici.

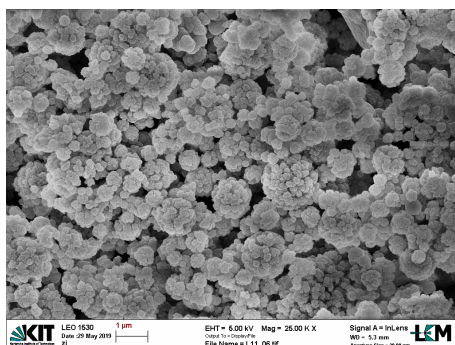
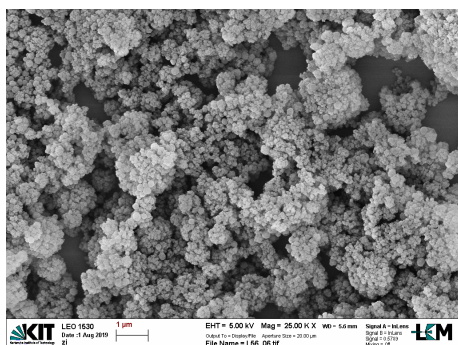
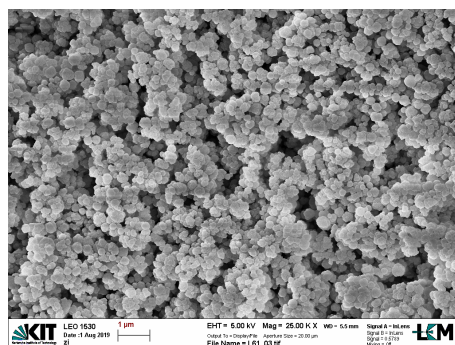


Figura 8: Immagine al FE-SEM di micro-particelle ottenute con meccanismo radicalico acrilico.

Al contrario dei tioli, con alcuni monomeri è stato possibile effettuare molti esperimenti senza l'aggiunta di co-solventi per via della più facile solubilità nei solventi precedentemente menzionati. Le varie strutture dei 5 monomeri sono state, poi, confrontate fra di loro nella stessa formulazione della soluzione spray: 10 g di esadecano e 15 grammi di isottanolo con un rapporto M/S pari a 29:71. Una struttura a mosaico, con particelle che ricordano la superficie di un cavolfiore, è stata ottenuta dalla polimerizzazione di TMPTA. Negli altri casi si sono ottenute delle strutture polimeriche disgregate parzialmente (nel caso di HDDA) e totalmente (nel caso del Neopentyl) dove le particelle non sono più distinguibili. Entrambi i monomeri però formano una matrice disgregata anch'essa caratterizzata da domini polimerici dell'ordine di decine di nanometri, leggermente più evidenti dei precedenti prodotti da TMPTA.



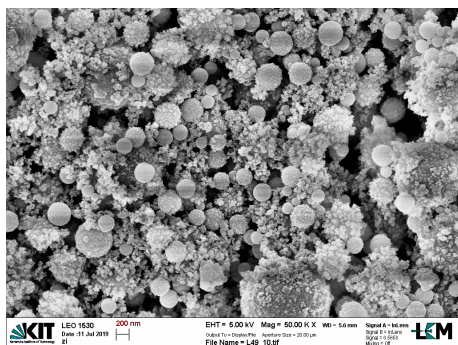
(a) Matrice polimerica data da HDDA.



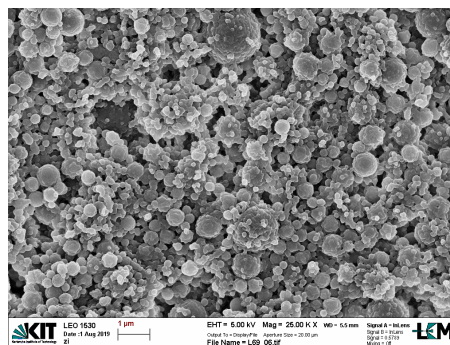
(b) Matrice polimerica data da Neopentyl.

Figura 9: Immagini al FE-SEM delle matrici polimeriche ottenute con meccanismo acrilico.

Come precedentemente effettuato, è stato valutato l'effetto dei diversi tipi di co-solvente, cioè dell'aggiunta di una sostanza con volatilità diversa alla soluzione spray. Il rapporto M/S è stato mantenuto costante al valore di 20:80 con 10g di esadecano, 10g di isottanolo e 20g di co-solvente utilizzato fra acetone, etanolo e 1-propanolo. In alcune serie di esperimenti sono



(a) PETA in presenza di etanolo.



(b) TMPe7TA in presenza di 1-propanolo.

Figura 10: Immagini al FE-SEM delle micro-particelle decorate ottenute con meccanismo acrilico.

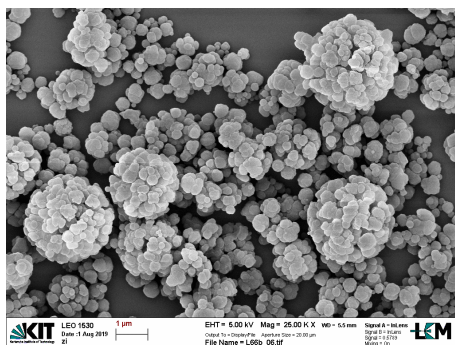
anche stati testati i monomeri PETA e TMPe7TA laddove la soluzione si presentava omogenea con la composizione appena menzionata.

Nonostante la leggera diminuzione del rapporto M/S, la morfologia delle particelle è rimasta pressochè identica a quella ottenuta senza l'aggiunta di co-solvente. La dimensione delle particelle e dei domini polimerici che caratterizzano la superficie, invece, è variata di una quantità poco apprezzabile. Ciò è dovuto alla presenza di una sostanza molto più volatile degli altri solventi utilizzati, che contribuisce ad aumentare la frazione di vuoto creata dopo la sua evaporazione e ritarda leggermente la separazione di fase fra le sostanze nella goccia.

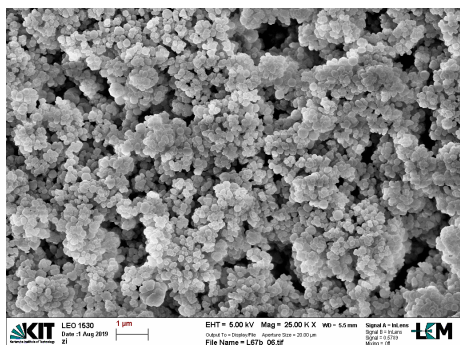
Micro e nano-particelle sferiche decorate con domini polimerici simili a quelli precedenti sono state ottenute dalla polimerizzazione di PETA in presenza di etanolo. La distribuzione dimensionale di queste particelle, come si può evincere dalla Figura 10a, è però molto ampia: le dimensioni spaziano da qualche centinaia di nanometri a 1,5 µm circa. Una distribuzione dimensionale simile è stata ottenuta con il monomero TMPe7TA in Figura 10b, dove però la struttura appiccicosa è caratterizzata da particelle corrugate interconnesse da ponti.

La scelta del monomero si è rivelata strettamente legata al numero di gruppi funzionali che possiede: da questa variabile dipende la velocità di polimerizzazione e la capacità di creare strutture ramificate nello spazio o lineari. Monomeri trifunzionali o tetrafunzionali hanno prodotto particelle distinguibili e strutture dettagliate e ben definite nonostante la bassa quantità di reagente presente in soluzione. Mentre, monomeri bifunzionali, come Neopentyl e HDDA, non hanno un'elevata possibilità di creazione di conformazioni differenti nello spazio per via della limitata disponibilità di gruppi radicali sulle estremità della catena polimerica. Ciononostante, particolari caratteristiche intrinseche di un monomero (come peso molecolare o polarità della molecola) possono portare alla formazione di particelle non distinguibili anche con alti numeri di gruppi funzionali (caso TMPe7TA).

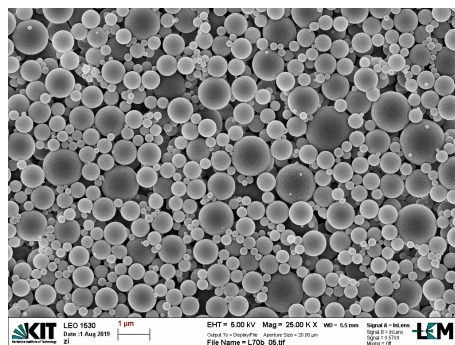
Oltre al co-solvente, è stato valutato anche l'effetto degli altri solventi presenti in soluzione. Data la poca influenza del co-solvente sulla morfologia delle particelle, i risultati qui menzionati sono stati basati sul parametro M/P (rapporto monomers-to-porogens). L'aggiunta di esadecano nella soluzione contenente TMPTA ha portato alla formazione di particelle più corrugate e avvizzite diminuendone anche la dimensione (struttura a mosaico più accentuata). Le prove condotte con HDDA in presenza di 1-propanolo hanno permesso di ottenere varie strutture: particelle corrugate con nano-domini polimerici con un rapporto M/P di 50:50, una matrice disgregata con un rapporto M/P di 33:67 e infine particelle piene e sferiche con il solo impiego del monomero disciolto nel co-solvente.



(a) HDDA con M/P pari a 50:50.



(b) HDDA con M/P pari a 33:67.

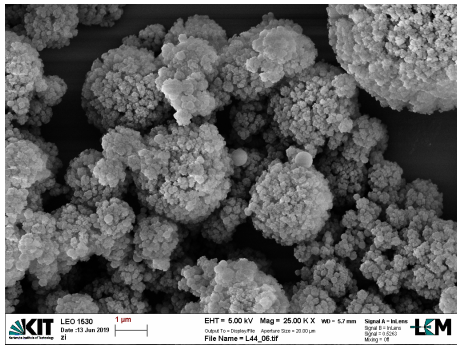


(c) HDDA in sola presenza di 1-propanolo.

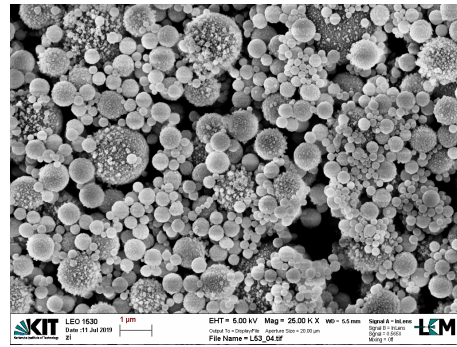
Figura 11: Immagini al FE-SEM di micro-particelle ottenute al variare del rapporto M/P.

Prove simili sono state effettuate anche variando esclusivamente la quantità di isoottanolo aggiunta. La serie condotta sia per TMPTA che per HDDA ha fornito gli stessi risultati, dimostrando che la morfologia dipende dal rapporto M/P. La propagazione della catena è favorita per elevati rapporti M/P perciò con l'aumento della concentrazione di monomeri all'interno di ogni singola goccia nebulizzata e quindi la possibilità di interazione fra il monomero e il radicale. L'aumento di velocità di polimerizzazione favorisce la ramificazione della struttura polimerica e produce particelle di piccole dimensioni con una superficie liscia. Bassi valori di M/P invece caratterizzano la superficie della particella con domini polimerici nanostrutturati (o addirittura portano a disgregazione della matrice), ma producono particelle di dimensioni maggiori.

Una verifica anche sul ruolo di 2-ottanone è stata effettuata. Il suo ruolo non è fondamentale come per il meccanismo tiolo-ene, in quanto non è necessario sia la presenza di un buon solvente per stabilizzare la soluzione spray che il ritardo della gelificazione del polimero formato. I risultati mostrano come l'impiego di questo solvente in una soluzione di TMPTA in etanolo con un rapporto M/P pari a 33:67 e M/S pari a 20:80 diminuisca la quantità di domini polimerici sulla superficie delle particelle. Ritardando la separazione di fase all'interno della goccia, diminuisce il grado di strutturazione della superficie della particella e anche la sua porosità. La struttura a mosaico in Figura 12a viene smorzata ad una mera decorazione di nano-domini illustrata nella figura accanto.



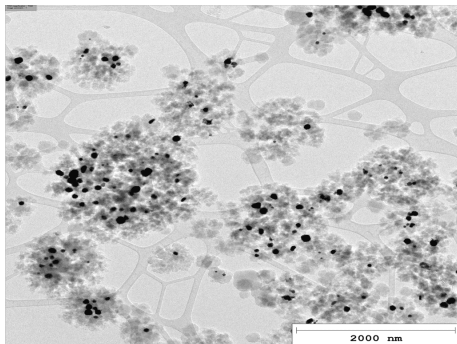
(a) TMPTA in assenza di 2-ottanone.



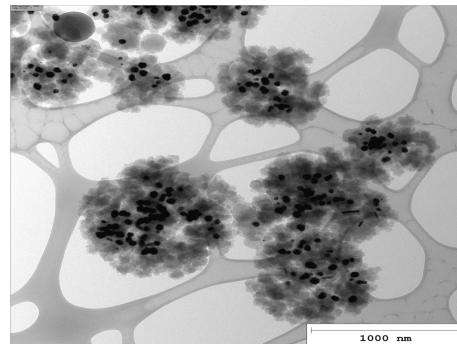
(b) TMPTA in presenza di 2-ottanone.

Figura 12: Immagini al FE-SEM di micro-particelle di TMPTA in eventuale presenza di 2-ottanone.

Per concludere, anche in questo caso sono state effettuate diverse prove per la creazione di particelle ibride. Tutte le soluzioni contenenti nano-particelle d'argento sono state impiegate anche per particelle di TMPTA e HDDA. In entrambi in casi, l'incorporazione ha avuto successo e gli esperimenti sono stati condotti perfettamente con l'utilizzo di inchiostro d'argento e della soluzione di nano-particelle disperse. Sono state prodotte micro-particelle ibride con struttura a mosaico sia nel caso di TMPTA con un rapporto M/P di 33:67 e 6 g di inchiostro (Figura 13a) e sia con stesso rapporto M/P e 3 g di soluzione di nano-particelle disperse. L'utilizzo di tetrafluoroborato di argento ha invece modificato la morfologia delle particelle polimeriche prodotte. Sebbene l'esito sia positivo, l'esperimento ha inoltre causato il blocco dell'atomizzatore con la formazione di una sostanza viscosa all'interno della soluzione sia nel caso di TMPTA che nel caso di HDDA, probabilmente per l'elevata reattività del sale. Nel secondo caso, addirittura, non è stato possibile prelevare un campione di materiale per le analisi. La scelta del composto è stata scartata, in quanto non adatto al processo.



(a) Particella ibrida di TMPTA e Ag.



(b) Particella ibrida di HDDA e Ag.

Figura 13: Immagini al TEM di particelle ibride ottenute con meccanismo acrilico.

0.4 Conclusioni

In questo lavoro sono stati analizzati i meccanismi di polimerizzazione radicalico acrilico e radicalico tiolo-ene per i quali si è cercato di produrre particelle piene, porose e a forma di capsula o a forma di caps. Oltre a ciò, sono stati valutati i principali parametri inerenti la composizione chimica della soluzione liquida e le apparecchiature utilizzate e come essi influiscano sulla morfologia e dimensione delle particelle ottenute. Per la prima volta sono state prodotte micro-capsule ben definite tramite il meccanismo tiolo-ene e nano-particelle a forma di caps sono state ottenute con l'aggiunta di glicerolo. Sono stati studiati i fenomeni coinvolti nel meccanismo riguardanti le specie reagenti e il ruolo dei solventi impiegati.

In merito al meccanismo radicalico acrilico sono state prodotte micro e nano-particelle con struttura a mosaico ad elevata area superficiale e sono state studiate le cause della modifica della loro superficie. I principali risultati influenti su questo meccanismo differivano da quelli che hanno influenzato il meccanismo tiolo-ene.

Infine, è stata studiata la possibilità di produrre strutture ibride tramite incorporazione *in situ* di particelle di argento nella matrice polimerica. L'esito è stato positivo con l'utilizzo di particelle di 50 nm nella matrice polimerica acrilica e negativo nei tentativi effettuati con il meccanismo tiolo-ene.

Ciononostante, molteplici studi potranno essere condotti per apprendere meglio le differenze fra i due meccanismi trattati. Alcuni esperimenti hanno mostrato problemi di adattabilità al processo e alcune cause non sono ancora ben definite. Nel futuro potranno essere ricercate nuove composizioni della soluzione spray e nuove apparecchiature con caratteristiche di funzionamento differenti, capaci di modificare le strutture polimeriche ottenute sulla base dell'applicazione a cui sono destinate.

Chapter 1

Introduction

1.1 Overview of microscaled and nanoscaled systems

Nowadays, microscaled polymer particles are diffusely employed in many applications in technical and biomedical fields, e.g. in medical research, immunological analysis, biological separation, chromatographic and catalytic supports and modelling of physical phenomena (Esen and Schweiger, 1996). The main reason is due to that they can be easily formed and designed by choosing the correct production technique and the proper polymeric material.

The term "microparticle" refers to a spherical particle whose diameter varies in the micrometer range (1 μm to 1000 μm) (Campos et al., 2013). With regard to nanoparticles, instead, their diameter varies from 1 nm to 1000 nm, although the range generally obtained is 100–500 nm. They contains from 20 to 15000 atoms and exists in a realm that straddles the quantum and Newtonian scales (Liu, 2006).

The first application in the industrial field for microparticles dates back to 1953. It consists of a carbonless copy paper, developed by L. Schleicher and B. Green. This improved copying paper was obtained by undercoating sheets of paper with microcapsules containing a colourless dye precursor. Then, in 1970, W.M. Holliday and collaborators patented the use of microparticles in the pharmaceutical industry for the first time, as an orally administered. Acetylsalicylic acid was encapsulated in a microcapsule made up of ethyl cellulose (Holliday et al., 1970).

When an active compound is immobilized into them, polymeric microparticles can be usually distinguished in "microspheres" and "microcapsules". "Microspheres" refers to microparticles composed of a homogeneous mixture of active compound and raw material, whilst the word "microcapsules" encloses all the microparticles with a liquid, solid or gaseous core in which the active compound is placed, covered by a layer of raw material (Campos et al., 2013).

This concept, of microparticles as encapsulation systems, was already drawn up in 1932 by the Dutch chemist H.G. Bungenberg. He used the term "coacervate" to describe the structure of a droplet containing a colloid surrounded by a tight layer of water, providing a locally segregated environment (Bungenberg, 1932). In the last decades, microencapsulation has been especially exploited with peptides and proteins, since they are very active in small doses, available in small quantities, sensitive to unfolding in organic solvents and minimum variations of environment conditions and, moreover, very expensive. Additionally, some of new synthesized molecules have poor solubility in aqueous or lipidic media and need protection during carriage through different systems (Benita, 2005).

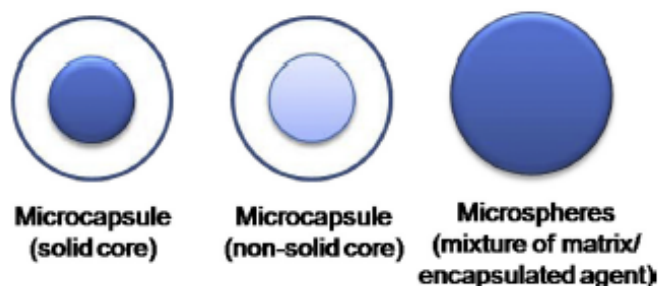


Figure 1.1: Categories of microparticles. Figure adapted from (Campos et al., 2013) with modification.

Also for nanoparticles, a distinction between nanospheres and nanocapsules is made which definitions are practically the same as for microspheres and microcapsules (Fattal and Vauthier, 2002). Nanoparticulated systems are investigated as active vectors due to their capacity to release drugs (Cruz et al., 2006). In particular, their subcellular size favours a higher intracellular absorption than other particulate systems (Furtado et al., 2001). They can improve the stability of the encapsulated substance and can be biocompatible with tissues and cells whether created from biocompatible materials (Guinebretière et al., 2002). Other advantages of nanocapsules include high drug encapsulation efficiency thanks to drug solubility in the core, drug polymeric protection by the shell against degradation factors and low polymeric content compared to nanospheres or other tiny-particulated systems (Pinto et al., 2006; Anton et al., 2008).

1.2 Production of micro and nanoparticles

In the last century, several techniques have been performed and improved for production of micro and nanoparticles. Monodisperse polymer microspheres have been usually prepared via conventional techniques of emulsion or suspension polymerization, but recently, photopolymerization reactions in aerosol have been investigated (Esen et al., 1996). It represents an alternative way to liquid-based methods.

Photo-initiated polymerization has been exploited for several purposes such as study of non-steady state polymerization kinetics, detection of photochemically produced free radicals and electrophoresis of biological substances. The main reason why this process is suitable to many applications is that no elevated temperatures are required (Oster and Yang, 1968).

Although the reaction occurs in a photo-induced process, nanoparticles can be synthesized in a liquid or in a gas phase. In this thesis, the aerosol technique was treated, due to some observed advantages in the overall process: a high purity of the product, the ability to produce micro and nanostructures in a continuous process and the reduction of waste generation. In fact, liquid routes are often batch processes in which impurities cannot be totally removed and require a remarkable amount of solvents. All these advantages foster this technique an appetite for industrial fields and large-scale productions (Biskos et al., 2008).

In addition, there are more benefits linked to the mechanism of aerosol photopolymerization:

- the ability to easily produce thin polymer films or layers onto a desired substrate,
- the size of the particle formed depends on the size of the droplet sprayed by the atomizer thereby making it handily manageable,
- possibility to combine different monomers and create homogeneous droplets which contain reactants and solvents,
- the control of residence time of each droplet in order to reach the desired polymerization rate

- the capability to generate hybrid particles *in situ* with addition of additives in the spray solution.

There are in total two methods to produce micro and nanoparticles. The former consists of the atomization of a liquid solution into droplets that crystallizes following the evaporation of the solvent; the latter, so called gas-to-particle conversion, consists of evaporation of the solution, including reactants and solvents, upon consequent nucleation and condensation in a inert gas phase. After heating the system up to let the substances evaporate, by using furnace, flame, plasma or laser reactors, glowing wires and spark discharges, there is a controlled cooling of the gas-vapor system that cause the above-mentioned condensation (Biskos et al., 2008).



Figure 1.2: The whole employed setup: on the left the pneumatic atomizer connected to the 4-FEP tube photoreactor (on the right).

In this thesis, the liquid solution was sprayed by pressurized nitrogen, using a pneumatic method. This is the ideal method for production of particles in the nanotechnology area, together with the ultrasonic and the electrospray atomization.

The pneumatic atomization works by exploiting a pressurized air stream which flows through a nozzle. After the expansion it keeps moving perpendicularly towards the end of a tube connected to the liquid vessel. The liquid is drawn due to the Bernoulli effect, which high difference of pressure created between the two phases breaks the continuous liquid phase into small droplets. The spray stream created conveys the droplets onto an impactor that let only the smaller droplets exit the atomizer, whilst the larger ones are sent back to the same liquid vessel or in another part of the apparatus, in accordance with its design (different models are described in Section 2.2). Generally, this method allows to produce particles in the size range of 1-10 μm (Biskos et al., 2008).

Another way to create microscaled droplets is by ultrasonic vibration of the air-liquid interface through a piezoelectric crystal. Boguslavskii and Eknadiosyants (1969) combined both mechanisms: drop formation is initiated by formation of capillary waves and driven by break-up of cavitation bubbles (Boguslavskii and Eknadiosyants, 1969). Droplets produced are function of the frequency of vibration and the physical properties of the solution. This technique produces high mono-dispersed particles and at the same time a low particle number concentration. In

addition, the atomizer is not always stable (Biskos et al., 2008).

The last method above-mentioned is the electro-hydrodynamic atomization (EHDA), namely, electro-spraying that produce droplets by exploiting electrical forces. By monitoring the liquid flow rate and the electrostatic potential between the liquid and the counter electrode, a large variety of droplets can be produced, from nanoscaled sizes to a few micrometers. The risk of nozzle clogging, here, is reduced and moreover is possible to control the trajectory of the produced droplets through the columbic forces. Nevertheless, this technique does not allow to achieve a large-scale production that hinders implementations in industrial processes (Biskos et al., 2008).

Once that the solution droplets are dispersed in the continuous nitrogen flow, they can go through the photoreactor where UV can activate the photosensitive substances. This avoids the employment of surfactants, as happens for other polymerization techniques, instead (Esen and Schweiger, 1996). Details of the setup and equipment used in this thesis are explained in Chapter 2.

1.3 Mechanisms of polymerization

Polymerization mechanism can be divided into step polymerization and chain polymerization. In the first mechanism, monomers gradually grow to dimers, trimers, tetramers and oligomers. Thus, the speed rate of the reaction is slow and the chain molecular weight increases slowly. The reaction can basically occur between any involved species. The thiol-ene mechanism treated is based on step-growth polymerization.

In chain polymerization, instead, an initiator (photoinitiator in this case) is needed to start the reaction. The creation of a reactive center promotes the further chain growth and it may be a free radical, a cation or an anion. Monomers start to be added through the active center which every time is shifted to end of the chain, so propagation phase can occur. Therefore, in this case, only a single monomer at a time can be added to the chain, but the active center moves fast and polymer chain weight increases faster. The acrylic radical polymerization is included in this category of mechanisms, which is the one compared to the thiol-ene polymerization, in the work.

1.3.1 Thiol-ene radicalic step-growth polymerization

The first part of the discussion of the results is about reactions between multi-functional thiols and ene-monomers through a step-growth mechanism. For the first time, Kharasch et al., in 1938, proposed a path to explain how this reaction occurs (step 1-4) and even now, it is still accepted.

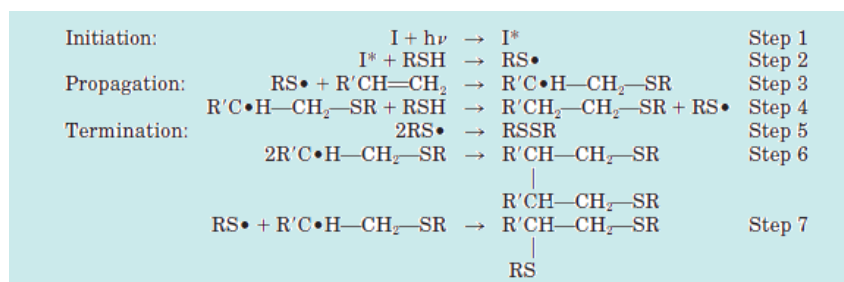


Figure 1.3: Thiol-ene mechanism. Figure adapted from (Cramer and Bowman, 2001) with modification.

As it is shown in the last scheme, it is well known that monomers cannot homopolymerize. This reaction leads to the formation of a cross-linked polymeric matrix with delayed gelation point and low volume shrinkage. The wide choice of ene-monomers which can be combined with each thiyl radical permits to manufacture a large variety of structures with different physical and mechanical properties for many applications.

Nevertheless, there are important drawbacks such as limited shelf-life stability (which life can vary from few seconds to few weeks) and bad odour of the thiol. Moreover, the presence of oxygen involves the addition of a chain transfer to the overall reaction. Some stabilizers in order to extend the shelf-life thiol-ene mixtures and multifunctional low-odor thiols have been further investigated to counteract these problems (Esfandiari et al., 2013).

The initiation includes two steps: in the first reaction the formation of an excited molecule of photoinitiator occurs (I^*). A thiol functional group (RSH) of the system reacts with the excited molecule thereby extracting a hydrogen and creating a thiyl radical ($RS\cdot$).

The propagation step involves two reaction as well. The formed radical reacts with ene-monomer and chain growth can start. Generally, both monomers involved are consumed in a ratio equal to their stoichiometric rates, but Cramer and Bowman (2001) noticed that in thiol-acrylate polymerization, conversion of acrylate monomers was approximately twice that of thiol functional groups.

At the end, the termination of a polymeric chain can occur either by a recombination of two radical groups or by a radical recombination with initiating species (Cramer and Bowman, 2001).

1.3.2 Acrylic radicalic chain-growth polymerization

Also this mechanism can be divided into sequence of three macro-steps.

In the initiation step two reaction are involved. One molecule of photoinitiator produces two free radicals by homolytic scission with a specific dissociation rate coefficient k_d . In this thesis, Irgacure 907[®] was employed in both mechanism of polymerization and Figure 1.4 represents the decomposition of this molecule through UV radiation. The first radical formed is called primary radical and it is the one that starts the chain growth.

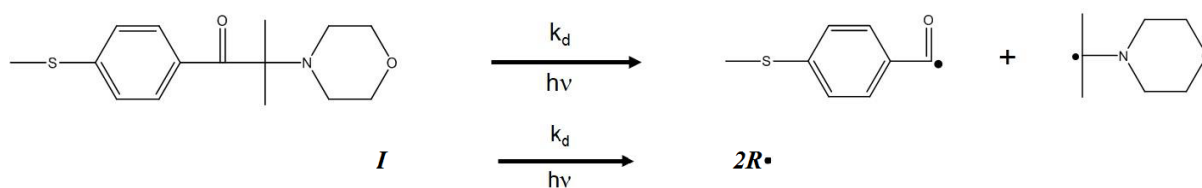


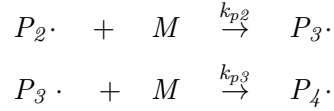
Figure 1.4: Decomposition of Irgacure 907[®] into two free radicals and the summerized reaction.

In fact, this radical is added to the acrylic monomer which reaction consists in the second phase of the initiation step. $P_i\cdot$ represents the polymeric chain composed of i bonded monomers (called primary monomer radical) and k_i is the rate coefficient for this reaction of initiation.



Subsequently, monomers add one at a time to the growing chain and proceed as indicated in the reactions below:



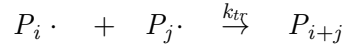


This series of reaction constitutes all the propagation step which can be summarized in the following general reaction:



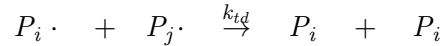
where k_p is the propagation rate coefficient. The value of this parameter is usually between 10^2 and $10^4 \text{ L mol}^{-1} \text{ s}^{-1}$ or even above for most monomers, making this mechanism faster than the step-growth mechanism (Akgün et al., 2014). After every monomer addition, the active center is moved to end of the chain.

Stop of the growth (termination step) can occur either by recombination or by disproportionation. The former produces larger dead polymer chains through reaction between free radical ends of two different chains. The reaction is shown below:



where k_{tr} is the termination by recombination rate coefficient. Dead polymers are no longer able to grow to larger chains.

The latter occurs when a hydrogen radical *beta* is transferred to another radical center of another polymeric chain. After that, a saturated polymer molecule and one unsaturated are formed. In the reaction below, k_{td} is the termination by disproportionation rate coefficient.



In each case the chain polymer molecule is larger enough to achieve a thousands of grams per mole in molecular weight. Despite of the presence of the primary free radical formed by the photoinitiator, properties of the final polymer product are not influenced and the product can be considered almost pure and clean. The disproportionation leads to lower molecular weight and needs a fourth kind of reaction to transfer an hydrogen atom from one radical molecule to the second one. Hence, termination by disproportionation is less probable compared to recombination. It could be enhanced by chain transfer agents, to monomer, to polymer, or to solvent. In chain transfer agents at least one weak chemical bond is required which allows the occurrence of the reaction. The radical reactive center of the polymeric chain is transferred to another radical species, mostly less active than the previous one (Akgün et al., 2014).

1.4 The aerosol photopolymerization technique in the scientific literature

In the first half of the 1990s, over 4000 distinct references about aspects of photo-induced technologies were reported per year as a result of huge published works and papers activity in this field. Photopolymers are used in electronic materials, printing materials, optical and electro-optical materials, adhesives and coating materials, fabrication of devices and polymeric materials (Peiffer, 1997).

Photoinitiated polymerization was firstly used in the beginning of 1900 when Berthelot and Gaudechon polymerized ethylene by UV radiation. By now, the technique has evolved since 1996, when Esen and Schweiger produced highly monodisperse polymer particles with diameters of 5 to 50 μm . They generated multiacrylate monomer droplets by a vibrating-orifice droplet generator carried away by a pure nitrogen flow in reaction tube irradiated by UV light (wavelength of 360 nm). The whole reacting environment was devoid of oxygen to avoid any inhibition of radicals. The particles formed were spherical with a smooth surface (Esen and Schweiger, 1996).

Subsequently, microcapsules of a size in the range 10-50 μm with different shell thickness to core diameter ratios were produced by Esen et al., in 1997. This time, the liquid solution was composed of three substances: an acrylic-based photocurable resin which is the hydrophobic component, glycerol as hydrophilic component and a high-volatile mutual solvent which compound each droplet formed. Droplets were still generated by a vibrating-orifice aerosol generator and were illuminated with UV light to form a solid spherical polymer shell and a liquid core (Esen et al., 1997).

The influence of the solvent composition on morphology and dimension of polymer nanoparticles was also investigated by Raula et al., in 2004. Although this work does not totally concern this technique (because of the lack of a photo-induced process), it helped to understand in which way the co-solvent employed can affect production of nanoparticle through an aerosol synthesis of the droplets. Here, nanocapsules were prepared with and without a ketoprofen drug. The role the solvent was discussed using ethanol, THF, toluene and water, selected according to their capability to dissolve reactants and their vapor pressure (Raula et al., 2004).

An other remarkable work which laid the basis for this thesis was conducted by Akgün and his team. It is about a free radical photopolymerization for the production of spherical sub-micron polymer particles. The setup and the technique used were almost similar to that of this thesis: the photoreactor was a quartz glass tube which a XeCl excimer was placed in, able to irradiate the reacting environment with a quasi-mono-chromatic UV light at 308 nm of wavelength. The experiments produced spherical polymer nanoparticles and with a discussion of phenomena involved in the process (Akgün et al., 2013).

Aerosol-photopolymerization was also employed for the generation of organic-inorganic nanocomposites. With a similar experimental setup and the same photoinitiator used (Irgacure 907), ZnO nanoparticles were incorporated in a polymer matrix successfully. Moreover, the same hybrid nanoparticles were produced without a conventional photoinitiator by exploiting the UV absorptivity of ZnO nanoparticles only (Akgün et al., 2014).

Thereafter, Shaban and his team tested this technique for production of amphiphilic copolymers. Polyacrylamide, polystyrene and hydrophobically modified polyacrylamide were produced after spraying monomer droplets by an atomizer in a reactor with a residence time of about 30 s. Composition and morphology of the obtained nanoparticles were analysed: polyacrylamide par-

tics showed a cauliflower-like structure, while polystyrene particles showed basically a smooth surface (Shaban et al.,2016).

In 2017, through the cationic polymerization mechanism, micro- and nano-particles were produced via an aerosol photo-induced process. As done for this thesis, a liquid solution composed of solvents and reactants was sprayed and irradiated with UV-light during the reactor passage. By adjusting the formulation of the starting solution, different morphologies could be achieved (Bazzano et al., 2017). In the following chapter, a description about the procedures used for the experiments conducted in this thesis is provided.

1.5 Aim of the work

In this treatment different mechanisms of polymerization will be debated. The attention is focused on differences between step polymerization and chain polymerization in an aerosol-based process through a photochemical method. The aim of the work is to create and optimize an experimental setup that allows to generate nanostructured polymeric particles. Moreover, composition of the spray solution has been analysed and how it can affect nanoparticles size and morphology. Considering the results achieved by studies conducted the previous years, the plan of the work has been structured in two different sections: the former treats production of polymeric particles via a thiol-ene mechanism of polymerization, the latter via radicalic polymerization using acrylic monomers.

Chapter 2

Experimental section

2.1 Materials

Several chemicals were used to conduct experiments in this work such as: reactants (basically monomers), porogens, solvents, photoinitiators and inhibitors. Details of each compound used are given below:

- **Thiol-monomers provided by THIOCURE[®]:**

- Thrimethylolpropane Tri(3-mercaptopropionate), TMPMP
- Ethoxylated-Thrimethylolpropane Tri(3-mercaptopropionate), ETTMP 700
- Ethoxylated-Thrimethylolpropane Tri(3-mercaptopropionate), ETTMP 1300
- Glycol Di(3-mercaptopropionate), GDMP
- Glycol Dimercaptoacetate, GDMA
- Pentaerythritol Tetra(3-mercaptopropionate), PETMP
- Tris[2-(3-mercaptopropionyloxy)ethyl] isocyanurate, TEMPIC

- **Ene-monomers:**

- Trimethylolpropane triacrylate, TMPPTA, density of 1.1 g/mL at 25 °C, that contains 600 ppm monomethyl ether hydroquinone as inhibitor purchased from Sigma-Aldrich
- Diallyl Adipate, purity $\geq 98\%$, density of 1.02 g/mL at 25 °C, purchased from TCI
- Neopentyl glycol diacrylate, density of 1.031 g/mL at 25 °C, that contains 225 ppm monomethyl ether hydroquinone as inhibitor purchased from Sigma-Aldrich
- 1,3,5-Triallyl-1,3,5-triazine-2,4,6(1H,3H,5H)-trione, density of 1.159 g/mL at 25 °C, purity $\geq 98\%$ purchased from Sigma-Aldrich
- Tri(ethylene glycol) divinyl ether, density of 0.99 g/mL at 25 °C, purity $\geq 98\%$ purchased from Sigma-Aldrich
- Trimethylolpropane ethoxylate triacrylate, average molecular weight 428 g/mol, density of 1.11 g/mL at 25 °C purchased from Sigma-Aldrich
- Divinyl Adipate, purity $\geq 99\%$ stabilized with monomethyl ether hydroquinone purchased from TCI
- 1,2,4-Trivinyl cyclohexane, purity $\geq 98\%$
- 1,6-hexanediol diacrylate, density of 1.010 g/mL at 25 °C, purity $\geq 99\%$ stabilized with 90 ppm of monomethyl ether hydroquinone purchased from Alfa Aesar
- Pentaerythritol tetraacrylate, density of 1.19 g/mL at 25 °C, that contains 350 ppm monomethyl ether hydroquinone as inhibitor purchased from Sigma-Aldrich

- 1,4-Butanediol divinyl ether, purity $\geq 98\%$, density of 0.898 g/mL at 25 °C purchased from Sigma Aldrich
- **Porogens:**
 - Hexadecane, density of 0.773 g/mL at 25 °C, purity $\geq 98\%$ purchased from Sigma-Aldrich
 - 2-Octanone, density of 0.819 g/mL at 25 °C, purity $\geq 98\%$ purchased from Sigma-Aldrich
 - 2-Ethyl-1-hexanol, density of 0.833 g/mL at 25 °C, purity $\geq 99\%$ purchased from Sigma-Aldrich
- **Co-solvents:**
 - Ethanol ROTIPURAN[®], purity $\geq 99,8\%$ purchased from Roth
 - 1-Propanol ROTIPURAN[®] purity $\geq 99,8\%$ purchased from Roth
 - Acetone ROTISOLV[®], purity $\geq 99,9\%$ purchased from Roth
- **Silver:**
 - Silver tetrafluoroborate, purity $\geq 99,99\%$ purchased from Sigma-Aldrich
 - Silver ink, 50 wt.%, as a dispersion in tripropylene glycol mono methyl ether from Sigma-Aldrich
 - Silver dispersion, density of 1.45 g/mL \pm 0.05 g/mL at 25 °C with particle size ≤ 50 nm from Sigma-Aldrich
- 4-Methoxyphenol, purity $\geq 99\%$ purchased from Sigma-Aldrich used as inhibitor
- 2-Methyl-4'-(methylthio)-2-morpholinopropiophenone, Irgacure 907 purchased from Sigma-Aldrich used as photoinitiator
- Glycerol, purity $\geq 99\%$ purchased from Sigma-Aldrich

However, in this report, acronyms attributed to monomers might differ from the commercial ones just mentioned. At the end of the work a list of acronyms hereafter used is provided.

2.2 Equipment and instrumentation

Basically, the setup is made up of two main devices: an atomizer that sprays the prepared solution to produce micro droplets and a photoreactor in which the photochemical reaction occurs. The solution is prepared in a brown glass flask (Borosilicate, 100 ml) to avoid the triggering of photo-induced reaction within it. Once that the flask is screwed into the atomizer, a nitrogen line is open in order to start the process; the created aerosol stream contains a continuous nitrogen gas phase that conveys droplets through the photoreactor. Solution droplets are created utilizing a two-component nozzle able to reach diameter sizes around a micrometer and below. Through the manometer placed on top of the device nitrogen flow inlet pressure can be set and controlled. Concentration of the produced droplets is $10^7 - 10^8$ cm².

Throughout the work, two different atomizers have been used both based on the same injection principle:

- ATM 220 with different nozzles by TOPAS-GmbH: 1375, 2068, 2105, 2110 each of them with a diameter size of 0.3 mm.
- Aerosol Generator for Liquids UGF 2000 by PALAS-GmbH.



Figure 2.1: ATM 220 by TOPAS.



Figure 2.2: UGF 2000 by PALAS.

Both the atomizers let only droplets with size below $1\ \mu\text{m}$ pass through the photoreactor. The main difference between the two aerosol generators is the number of flasks used; in the first case the droplets bigger than $1\ \mu\text{m}$ are sent back again into the spray solution through another orifice placed on the side of the nozzle. In the latter case, these larger droplets are sent directly to another empty flask (the flask on the left shown in Figure 2.3,) avoiding the characteristic reflux observed on the flask wall in the first case. This could be an advantage since some photo-induced reactions might be triggered either during the preparation of the solution or during the spraying when the monomer droplet has not still left the flask. Therefore polymer particles might be accumulated in the flask and might clog the orifices of the nozzle. Whilst the nozzle of UGF 2000 by PALAS has less probability to be clogged, on the other hand unblock it has revealed quite challenging since all the components are not easily reachable. Hence, the first atomizer (Figure 2.1) has been the most used throughout the work.



Figure 2.3: Bottom of the aerosol generator by PALAS.

With regard to the photoreactor, three different models have been used. The first model consists of a 0.44 m quartz glass tube long with an inner diameter of 0.052 m (Figure 2.4). The second and the third ones have been built during the work.



Figure 2.4: Quartz tube photoreactor.

They consist of two and four FEP (Fluorinated ethylene propylene) tubes respectively, with a length of 0.57 m and an inner diameter of 0.14 m for each tube, which is the irradiated part. This material was chosen to lower the absorbance value to 0,55 AU, through the tube walls. The 4-tubes reactor has also an additional 0.74 meter long tube placed in between the two couples of irradiated tubes (shown in Figure 2.5b). This allows the aerosol stream to traverse both the couples of tubes from top to bottom, where final product is collected and this tube is not irradiated at all. Every model is surrounded by two arrays of three tubes that emits a poly-chromatic UV radiation. It ranges from 270 nm to 360 nm, with a peak emission of 312 nm.



(a) 2-tubes photoreactor.



(b) 4-tubes photoreactor.

Figure 2.5: The two type of FEP tube reactors.

Since most of the experiments were conducted at the pressure of 1 bar, residence time values are estimated considering the measured flow rate of 1,55 L/min given by all the nozzles used at that working pressure. Instead, in a few experiments in which the pressure was different, also the residence time might slightly vary. Specific details are reported in the Section 3.7.

For collection of the polymer produced by thiol-ene reactions, a coil plastic tube was used. The formed particles could adhere to the inner surface of the tube and then they could be collected with the help of a solvent once the experiment was completed. About the acrylate monomer reactions, a PTFE filter membrane having an average pore diameter of 100 nm has been preferred to the former collection method. Nevertheless it can be subjected to clogging, in a time that depends on both speed of the reaction and yield of the process. Thus, to avoid this problem, each membrane was substituted every 30 minutes.

Most of the experiments lasted exactly 1 hour. Taking into account both the speed of the reaction and the combination of monomer involved in the process, particularly for thiol-ene reactions, experiment duration was extended to 1 hour and 30 minutes or even 2 hours in order to collect a minimum amount of material to be analysed.

2.3 Analysis Techniques

Most of the images analysed in this paper are elaborated via a scanning electron microscopy. Scanning electron microscopy (SEM) is a microscopy technique which uses a focused beam of high energy electrons to process an image of the surface of the analysed sample. Field emission (FE)-SEM provides topographical and elemental information at magnifications that go from 10x to 300,000x, with virtually unlimited depth of field. Images are clearer, less electro-statically distorted and with an higher resolution. Samples need to be prepared before microscopy to resist to vacuum and high energy of the electron beam. The microscope which was used in this thesis was a high resolution field-emission scanning electron microscope (Leo Gemini 1530, Carl Zeiss, Oberkochen, Germany). It permitted to evaluate dimension and morphology of polymeric particles produced. Samples analysed were prepared as diluted suspension after having stirred overnight. This process is useful to break second agglomerates. A silicium wafer was used to absorb few micro-litres of this suspension. After drying, particles were coated (1-2 nm) with platinum or a mixture of platinum-palladium.

Transmission electron microscopy (TEM) was performed on a Philips CM 12 and a Zeiss TEM 912. The particles were brought on a TEM grid (Plano, S160-3, carbon film on 300 mesh Cu grid) after having prepared a similar diluted suspension as was done for SEM characterization.

Chapter 3

Results and discussion: Step polymerization

3.1 Variation of Ene-monomer

Exploiting the knowledge concerning the thiol-ene reactions achieved so far, some experiment were repeated to confirm the previous obtained results, at first. The combination TMPMP-TMPPTA was repeated with the recipe written in Table 3.1.

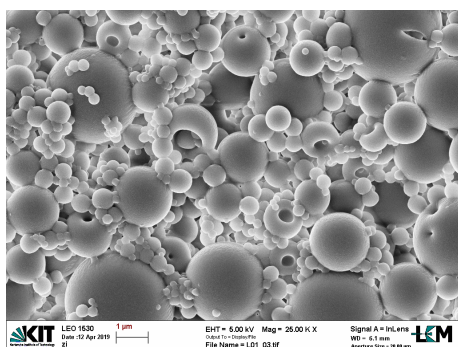
Instead, different combinations of monomers were tried for the first time. Then, they were compared each other in order to choose the most promising ones to produce nanostructured particles. A good number of experiments were performed, but only a few of them showed the minimum requirements that an aerosol process needs to avoid troubles concerning both the setup and the process itself.

Table 3.1: List of experiments with different ene-monomers used.

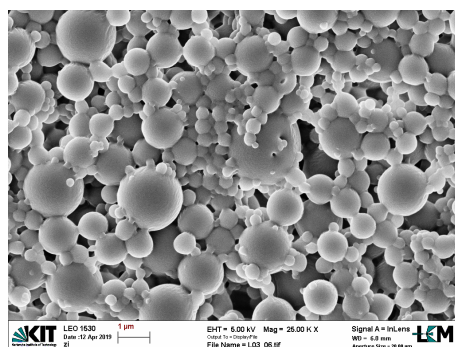
Exp.	Formulation spray solution						M/S Ratio	Molar Ratio	
	Reactants		Porogens			Co-solvent			Amount
			HD	2-Oct	IsoOct				
L01	TMPMP	TMPPTA	6,00	7,00	7,00	EtOH	20,00	33:67	1:1
L03	TMPMP	Diallyl	6,00	7,00	7,00	EtOH	20,00	33:67	1:1,5
L06	TMPMP	Triall-T	6,00	7,00	7,00	EtOH	20,00	33:67	1:1
L07	TMPMP	DVE	6,00	7,00	7,00	EtOH	20,00	33:67	1:1,5
L08	TMPMP	TMPe7TA	6,00	7,00	7,00	EtOH	20,00	33:67	1:1
L09	TMPMP	Neopentyl	6,00	7,00	7,00	EtOH	20,00	33:67	1:1,5
L12	TMPMP	DVA	6,00	7,00	7,00	EtOH	20,00	33:67	1:1,5
L23	TMPMP	TVC	8,00	3,50	3,50	EtOH	20,00	22:78	1:1

In each experiment above-mentioned, formulation was kept constant, varying only the ene-monomer. Keeping the molar ratio constant, the amount of the monomers was based on a total of 20 g. Only in the last experiment L23, the formulation differs from the the others, but this cannot modify the polymer structure extremely, as it is possible to see in the next subchapters. Despite the presence of good solvents such as 2-octanone and co-solvent that help to keep the solution homogeneous at the beginning and throughout the process, in most of the cases mixtures resulted turbid and heterogeneous. In some cases, phase separation took place quickly between components, even though the solution was stirred up for long times. In addition to the clogging of nozzles, the triggering of polymerization within the flask (as discussed in Section 2.2) reduces the solubility of the other components in the mixture while the solution is sprayed. As time passes, the more volatile the component is the more its amount in the flask is reduced, therefore,

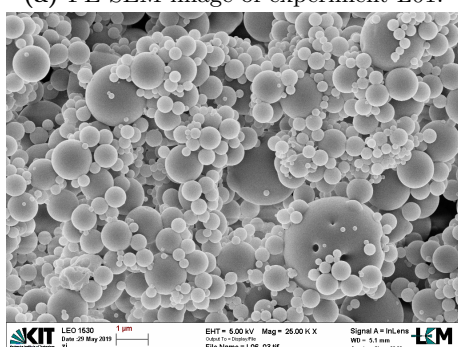
porogens and co-solvent will evaporate and the solution state could only be worse tending to a complete phase separation between every substance. For this reason, monomer combinations that involved such problems were treated no longer. Results are shown the following pictures.



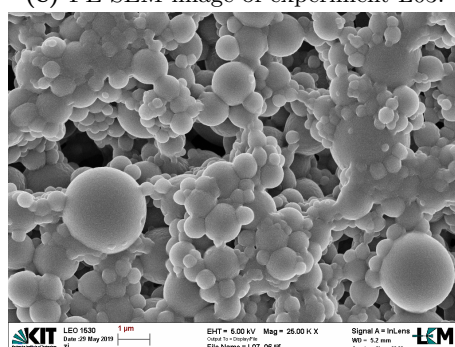
(a) FE-SEM image of experiment L01.



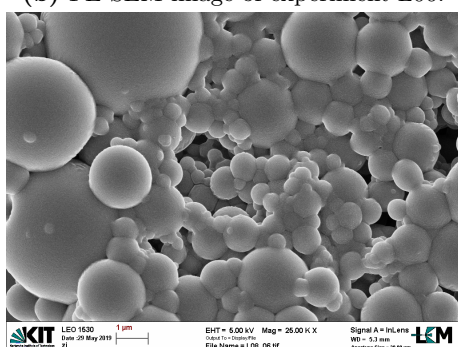
(e) FE-SEM image of experiment L03.



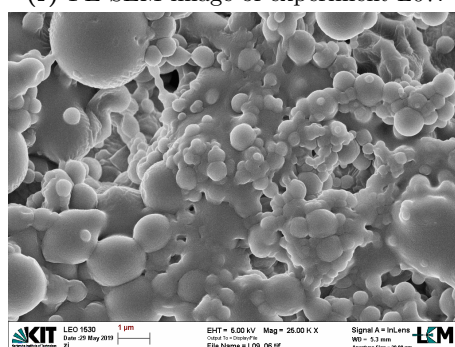
(b) FE-SEM image of experiment L06.



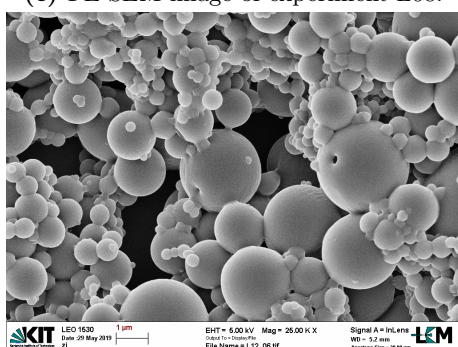
(f) FE-SEM image of experiment L07.



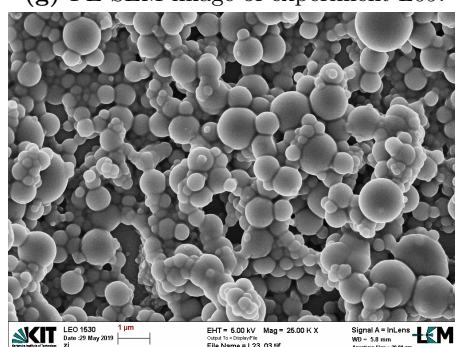
(c) FE-SEM image of experiment L08.



(g) FE-SEM image of experiment L09.



(d) FE-SEM image of experiment L12.



(h) FE-SEM image of experiment L23.

Figure 3.1: FE-SEM images of experiments described in Table 3.1.

Different morphologies were attained. Sponges and capsules are the typical ones for the thiol-ene reactions. Fundamentally, they differ from each other for the number of spotted holes on the surface of the particles. The former has more narrow irregular cavities (Figure 3.1b) inside, while the latter has one single bigger hole easily identifiable (Figures 3.1a, 3.1d). Once that the droplet passes through the photoreactor, the polymerization occurs and the substances that are not involved in the reaction still occupy the inner volume of the droplet. As polymer forms, the droplet is no more homogeneous and phase separation takes place thanks also to hexadecane that plays an important role in this step, as a bad solvent. Volatile components evaporate from the droplet forming cavities inside and on the surface of the particles. Therefore, the bigger is the droplet, the more is the volume occupied by porogens and so probability of their evaporation from different spots on the surface increases. Thus, in the figures above, only particles over 3 μm show a sponge-like structure (Figures 3.1e, 3.1b). Particles under about 1,5 μm are fully spherical and the intermediate ones have a capsule shape with one visible hole. For some of the combinations of monomer used, these differences cannot be seen because of the high stickiness of the polymer that could be an intrinsic property. These combinations have also been excluded because not in compliance with the aim of the work. The most promising structure was attained by the combination TMPMP - TMPTA of the experiment L01 (Figure 3.1a). Hence, the possibility of creating micro caps-like particles like those in the picture has been further investigated in the following experiments.

3.2 Variation of Thiol monomer

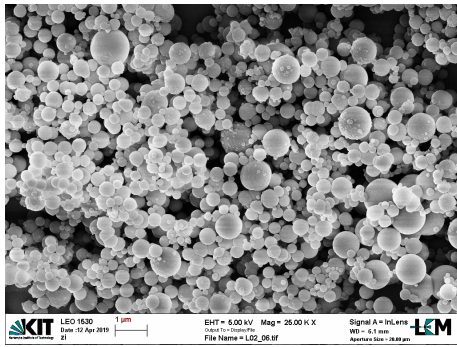
In order to choose the most promising monomers combinations, thiol monomers were tested as well. A series of experiments was performed with the selected ene-monomer TMPTA, taking into account parameters that should be respected to avoid arising problems, like those mentioned beforehand in the Section 3.1. The considered combinations are showed in the following table.

Table 3.2: List of experiments with different thiol-monomers used.

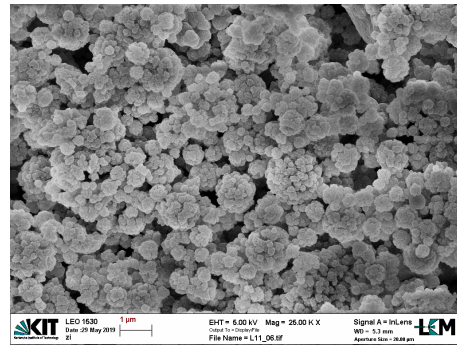
Exp.	Formulation spray solution							M/S Ratio	Molar Ratio
	Reactants		Porogens			Co-solvent	Amount		
			HD	2-Oct	IsoOct				
L02	TEMPIC	TMPTA	6,00	7,00	7,00	EtOH	20,00	33:67	1:1
L11	-	TMPTA	6,00	7,00	7,00	EtOH	20,00	33:67	-
L25	ETTMP700	TMPTA	8,00	3,50	3,50	EtOH	20,00	22:78	1:1
L26	GDMP	TMPTA	8,00	3,50	3,50	EtOH	20,00	22:78	1,5:1
L27	PETMP	TMPTA	8,00	3,50	3,50	EtOH	20,00	22:78	1:1,33
L28	GDMA	TMPTA	8,00	3,50	3,50	EtOH	20,00	22:78	1,5:1
L29	ETTMP1300	TMPTA	8,00	3,50	3,50	EtOH	20,00	22:78	1:1,33

Variation of thiol monomers has not led to relevant results, focusing just on the structure. As evidenced by the pictures, size distribution of the particles is what changes the most and particles are more or less individual depending on the composition of the polymer formed. Moreover, problems such as triggering of the reaction within the flask and compatibility of the substances have been occurred. Neither a single hole or a different conformation from the spherical shape is observed on particles surface, in spite of the presence of porogens. The lack of an homogeneous solution could be the main reason, since in these cases the sprayed droplet rarely contain all the substances which the solution is made up of (TEMPIC and GDMA were excluded for this reason). The amount of these porogens is neglectible to observe significant morphology effects. Most of these thiols were excluded from the discussion, whilst ETTMP 700 and PETMP were employed with different solvents (Section 3.3) and spray fomulations because of an interesting narrow size distribution and particles individuality (Figures 3.2b and 3.2c).

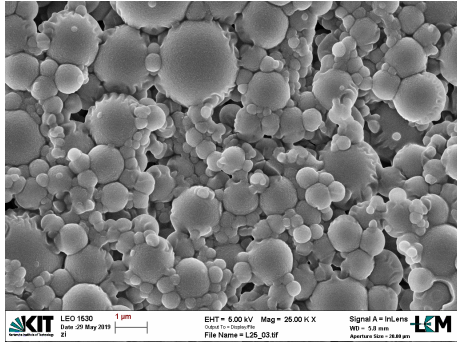
Speed of reaction between monomer plays an important role. Is ascertained that a thiyl radical does not react with another of the same type, only the acrylic monomer does. Knowing from the literature that the conversion of the two employed monomers is different (usually the ratio between conversions favours the ene-monomer), the polymer structure might depend on the speed of the thiyl radical formation reaction that compete with the formation of the other acrylic radical. The speed of the total reaction is linked to the number of functional group involved in the reaction; the more the functional groups are, the faster the reaction is, so keeping constant the three acrylic functional groups of TMPTA, the speed of the reaction increases with the decreasing of the molar ratio (in the Table 3.2). Bifunctionalized thiol monomers requires such a long time to polymerize that could by far shorter than the residence time of concerned system. For this reason, trifunctionalized and tetrafunctionalized thiol monomers have been preferred. Effect of the lack of a thiol monomer involved in the radicalic mechanism is showed in Figure 3.2d. A particular well detailed structure was obtained, characterized by a narrow particle size distribution and the presence of small nanodomains on the surface that sharply increases surface area of each particle. Concerning aspects of this mechanism will be treated in Chapter 4.



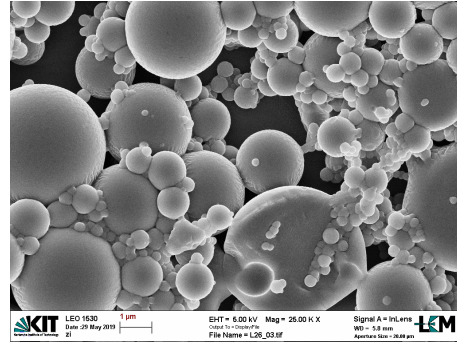
(a) FE-SEM image of experiment L02.



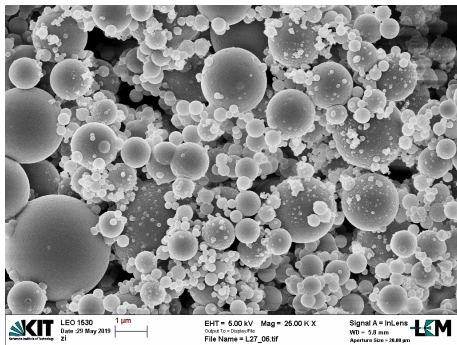
(d) FE-SEM image of experiment L11.



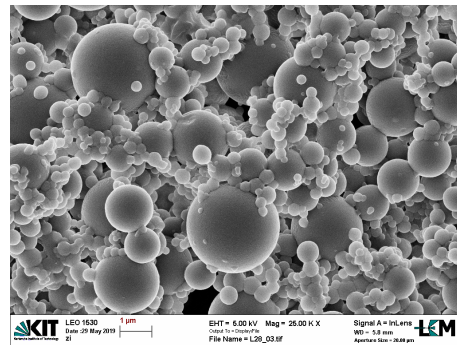
(b) FE-SEM image of experiment L25.



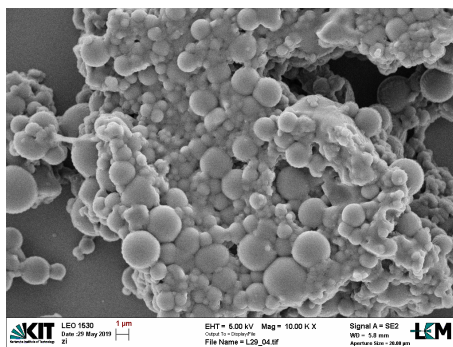
(e) FE-SEM image of experiment L26.



(c) FE-SEM image of experiment L27.



(f) FE-SEM image of experiment L28.



(g) FE-SEM image of experiment L29.

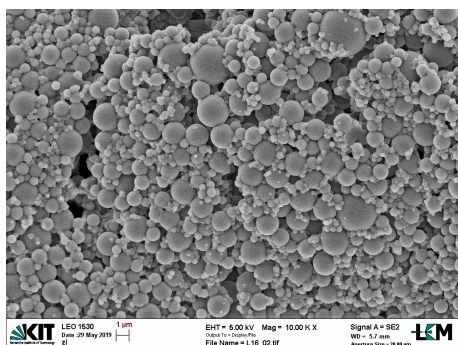
Figure 3.2: FE-SEM images of experiments described in Table 3.2.

3.3 Effect of different co-solvents

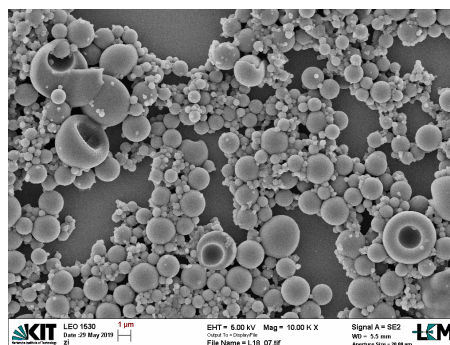
With reference to the encountered problems so far, different solvents were used to guarantee the homogeneity of the spray solution. Many experiments with acetone, 1-propanol, ethanol and no added solvent are compared below.

Table 3.3: List of experiments with different co-solvents employed.

Exp.	Formulation spray solution							M/S Ratio	Molar Ratio
	Reactants		Porogens			Co-solvent	Amount		
			HD	2-Oct	IsoOct				
L16	TMPMP	TMPTA	8,00	3,50	3,50	EtOH	20,00	22:78	1:1
L18	TMPMP	TMPTA	8,00	3,50	3,50	Acetone	20,00	22:78	1:1
L30	TMPMP	TMPTA	6,00	7,00	7,00	Acetone	30,00	29:71	1:1
L32	TMPMP	TMPTA	6,00	7,00	7,00	EtOH	30,00	29:71	1:1
L74	TMPMP	TMPTA	6,00	7,00	7,00	PrOH	30,00	29:71	1:1
L92	TMPMP	TMPTA	6,00	7,00	7,00	-	-	50:50	1:1



(a) FE-SEM image of experiment L16.



(b) FE-SEM image of experiment L18.

Figure 3.3: FE-SEM images of experiments described in Table 3.3.

In the first two pictures (3.3a and 3.3b) formulation was kept constant and only co-solvent was varied. As can be seen in the previous commented experiments, structure of the particles formed by TMPMP-TMPTA combination, in presence of ethanol as a co-solvent, is mainly chill with sporadic small holes spotted on particles bigger than 1 μm that confer the characteristic capsules-like shape. Instead, effect of acetone is much marked, especially on the biggest particles. This is due to the fact that acetone is much more volatile than ethanol so the evaporation of the co-solvent is easier and faster during the polymerization within the droplet. Also for this reason, the volume occupied by acetone in a droplet is greater than the one occupied by ethanol (considering the higher vapor pressure of the former) so bigger cavities let the collapse of the rounded particles more easily. In fact, this particular shape is not observed on smaller particles, in which the polymer is more rigid and does not collapse on its own weight. Another reason could be that the amount of acetone in nanosized particles is negligible, thus acetone can evaporate so fast that polymerization could take place in the entire volume of the droplet. In fact, as can be observed in the literature, solutions made up of reactants without additives, give chill-type particles with a smooth spherical shape, as the smallest particles in the pictures above look like. Thus, there is an interplay between this phenomena that might affect particles morphology. The polymer composition is contaminated when acetone is employed.

Keto-enol tautomerism of this solvent let the enol monomer work as a monovalent ene-monomer within the polymerization process.

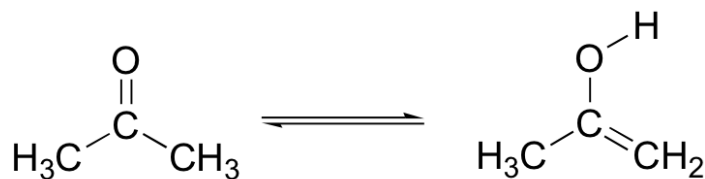
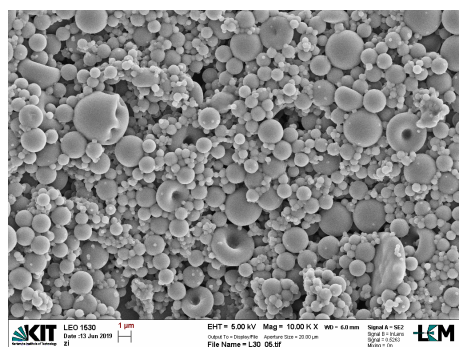
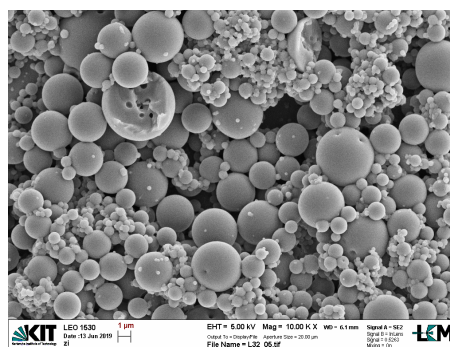


Figure 3.4: Keto-enol tautomerism of acetone.

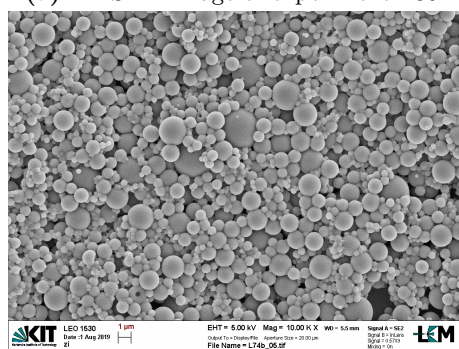
Since the enol monomers end the polymeric chain, they reduce the cross-linking of the structure which affects its morphology. The inhibition of possible reaction sites lowers the polymerization rate of the main reaction and it could be the responsible of a less rigid structure, due to the presence of irregular and non-organised clusters within the polymeric matrix. Entity of this phenomenon depends on the keto-enol tautomeric equilibrium and on polymerization rate of thiol-acetone reaction.



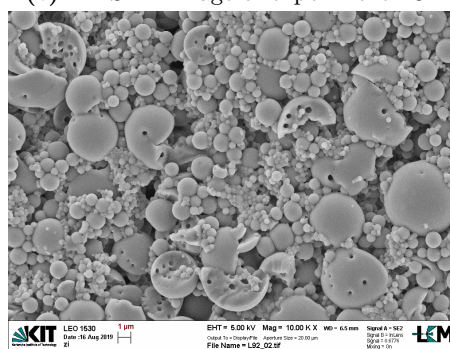
(a) FE-SEM image of experiment L30.



(c) FE-SEM image of experiment L32.



(b) FE-SEM image of experiment L74.



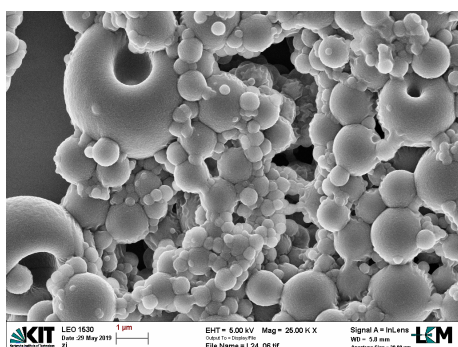
(d) FE-SEM image of experiment L92.

Figure 3.5: FE-SEM images of experiments described in Table 3.3.

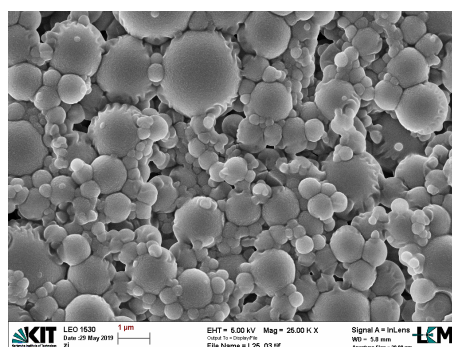
Despite different spray formulations, commented results can be confirmed comparing pictures above. Collapsed particles are observed for experiment with acetone, whereas the lowering of volatility of co-solvents produce particles more chill with random distributed pores. The absence of a co-solvent (Figure 3.5d) confirm the role of the porogens in the polymerization process, namely the achievement of a sponge-type structure. Variation of M/S ratio of such little amount does not lead to evident changes in the morphology like the slight different amount of porogens. The significant structural change is due to different co-solvents.

Table 3.4: List of experiments with different co-solvents employed.

Exp.	Formulation spray solution						M/S Ratio	Molar Ratio	
	Reactants		Porogens			Co-solvent			Amount
			HD	2-Oct	IsoOct				
L24	ETTMP700	TMPPTA	8,00	3,50	3,50	Acetone	20,00	22:78	1:1
L25	ETTMP700	TMPPTA	8,00	3,50	3,50	EtOH	20,00	22:78	1:1
L08	TMPMP	TMPe7TA	6,00	7,00	7,00	EtOH	20,00	33:67	1:1
L36	TMPMP	TMPe7TA	6,00	7,00	7,00	Acetone	30,00	29:71	1:1
L27	PETMP	TMPe7TA	8,00	3,50	3,50	EtOH	20,00	22:78	1:1,33
L39	PETMP	TMPe7TA	6,00	7,00	7,00	Acetone	30,00	29:71	1:1,33



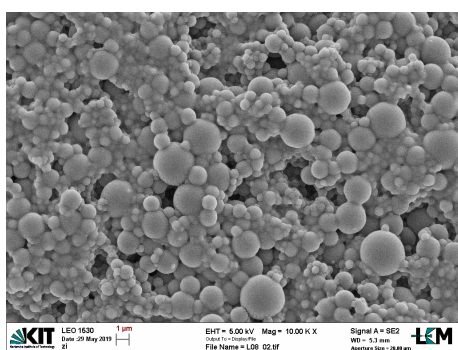
(a) FE-SEM image of experiment L24.



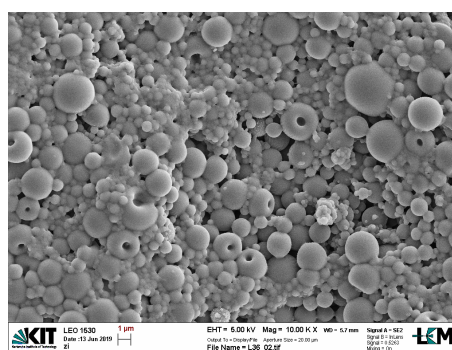
(b) FE-SEM image of experiment L25.

Figure 3.6: FE-SEM images of experiments described in Table 3.4.

As can be seen in the following pictures, the morphology strongly depends on the used co-solvent as well. In every case, acetone lead to capsule-like particles and ethanol rarely lead to collapse of polymeric outer surface. As discussed beforehand, the numerical density of the hollowed particles depends on how much the polymerization rate of the main reaction is influenced by the affinity of acetone to react with the thiol monomer, since the tautomeric equilibrium is constant in every experiment.

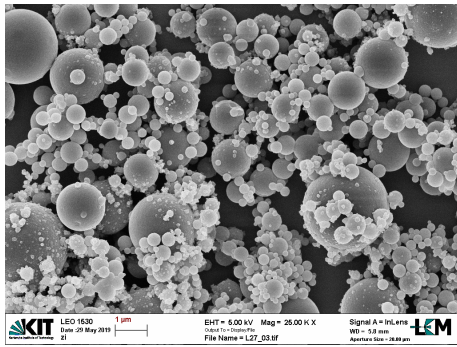


(a) FE-SEM image of experiment L08.

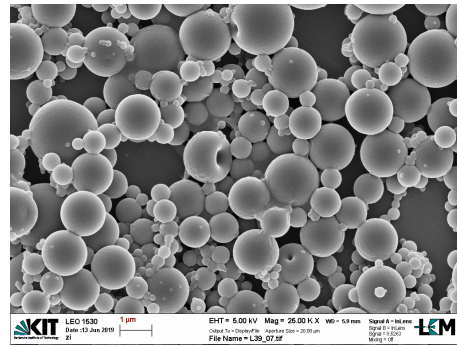


(b) FE-SEM image of experiment L36.

Figure 3.7: FE-SEM images of experiments described in Table 3.4.



(a) FE-SEM image of experiment L27.



(b) FE-SEM image of experiment L39.

Figure 3.8: FE-SEM images of experiments described in Table 3.4.

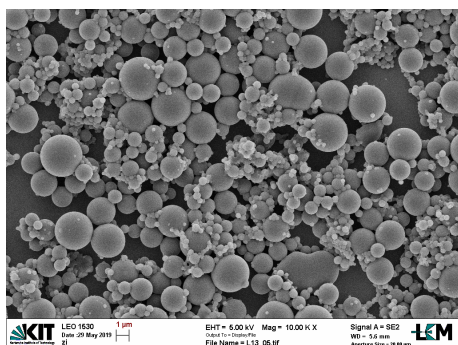
Choice of co-solvent in an aerosol photopolymerization process, when a step polymerization mechanism occurs, is a crucial step to guarantee the homogeneity of the spray solution and to modify morphology of particles significantly. The more volatile the co-solvent is, the easier the collapse of particles core shell is. To confirm this thesis, new solvents with both these characteristics should be experimented, avoiding parallel reactions or phenomena that could influence the main polymerization, since it has not been possible to evaluate how much they influence the process itself.

3.4 Effect of the amount of co-solvent

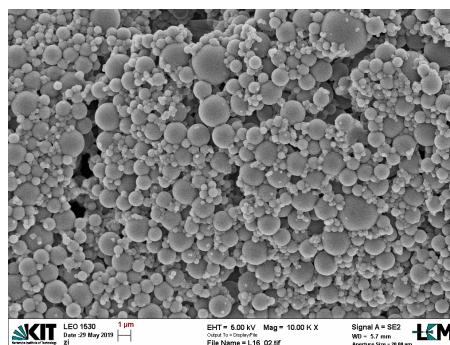
From SEM analysis, effect of the amount of co-solvent in spray formulation has been considered as well. The compared experiment are shown in the following table.

Table 3.5: List of experiments with different amount of co-solvents.

Exp.	Formulation spray solution							M/S Ratio	Molar Ratio
	Reactants		Porogens			Co-solvent	Amount		
			HD	2-Oct	IsoOct				
L13	TMPMP	TMPPTA	8,00	3,50	3,50	EtOH	10,00	29:71	1:1
L16	TMPMP	TMPPTA	8,00	3,50	3,50	EtOH	20,00	22:78	1:1
L01	TMPMP	TMPPTA	6,00	7,00	7,00	EtOH	20,00	33:67	1:1
L32	TMPMP	TMPPTA	6,00	7,00	7,00	EtOH	30,00	29:71	1:1
L92	TMPMP	TMPPTA	6,00	7,00	7,00	-	-	50:50	1:1



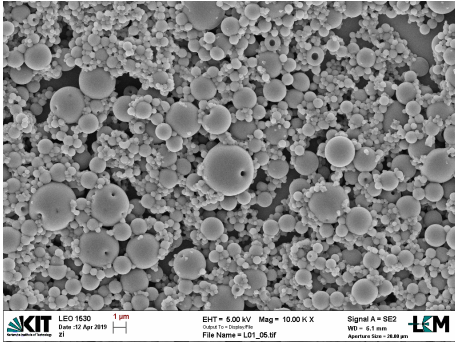
(a) FE-SEM image of experiment L13.



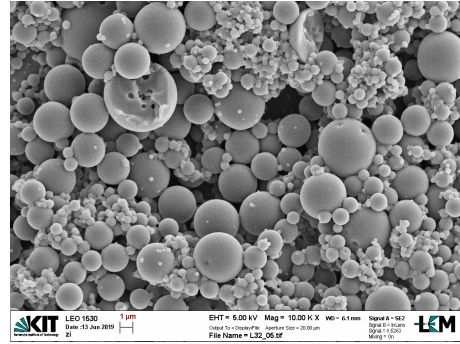
(b) FE-SEM image of experiment L16.

Figure 3.9: FE-SEM images of experiments described in Table 3.5.

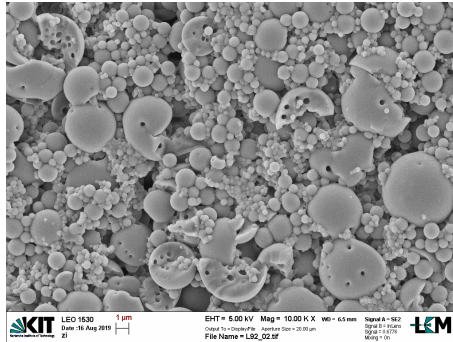
With regard to morphology, no considerable differences can be seen from SEM pictures. At a first glance, particle size distribution in Figure 3.9a look broader than the one of Figure 3.9b and particles are also more dispersed. Dispersion of the particles depends on the spreading of the sample on the silicon wafer used for SEM scanning, thus this does not concern any parameter of the experiment. The particle size distribution could be affected by the amount of co-solvent in the spray formulation, but looking at the pictures of the Figures 3.10a, 3.10b, 3.10c, no consideration can be drawn. In fact, with the increase of amount of co-solvent particles look bigger, but without co-solvent micro and nano particles are present at the same time. So this aspect could be affected also by the variation of the M/S ratio, which is the other non-constant parameter. Influence of this parameter will be treated in the following section.



(a) FE-SEM image of experiment L01.



(b) FE-SEM image of experiment L32.



(c) FE-SEM image of experiment L92.

Figure 3.10: FE-SEM images of experiments described in Table 3.5.

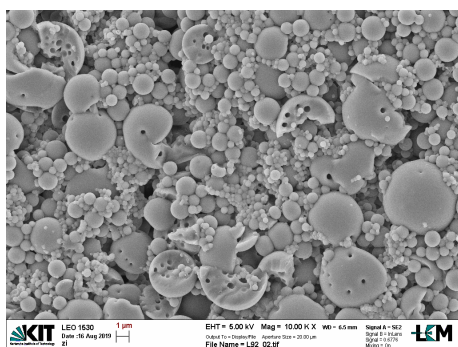
3.5 Effect of the variation of monomers to solvents ratio

Few experiments were conducted to truly show the effect of this ratio variation, so results could not be enough to demonstrate how strong the impact on a step mechanism reaction is. Two experiments without the usage of a co-solvent were performed and they are shown in the Table 3.6.

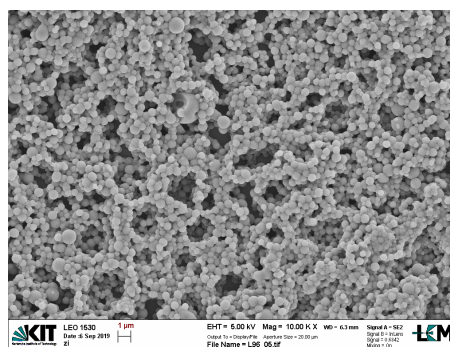
Table 3.6: List of the experiments without co-solvent and different amount of porogens.

Exp.	Formulation spray solution						M/S Ratio	Molar Ratio	
	Reactants		Porogens			Co-solvent			Amount
			HD	2-Oct	IsoOct				
L92	TMPMP	TMPTA	8,00	3,50	3,50	-	-	50:50	1:1
L96	TMPMP	TMPTA	15,00	17,50	17,50	-	-	29:71	1:1

Result of the experiment L92 has been already discussed in the previous section. The high amount of HD (as a bad solvent) anticipates phase separation and the presence of 2-Octanone and an alcohol is needed for production of porous particles, but looking at Figure 3.11b, particles obtained with the same substances are different.



(a) FE-SEM image of experiment L92.



(b) FE-SEM image of experiment L96.

Figure 3.11: FE-SEM images of experiments described in Table 3.5.

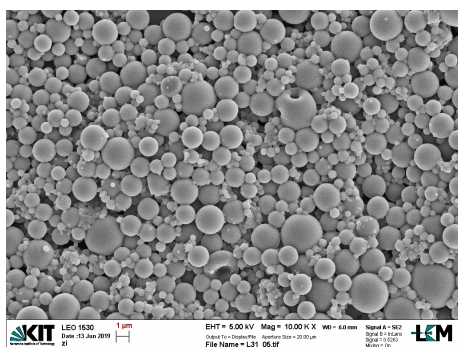
As discussed in the subsection 3.1, only particles with a diameter of 2-3 μm usually look porous and it is a matter of their size, primarily. For this reason, particles formed from the experiment L96 are not porous, showing that the M/S ratio affects the particle size. Moreover, they are more sticky and less individual due to the significant amount of 2-ethyl-1-hexanol and 2-Octanone. Considering that porogens are not as volatile as a co-solvent like ethanol or acetone, the droplet during the polymerization is still made up of all the substances contained in the flask and the evaporation will occur in a later moment. The amount of monomers able to polymerize within the droplet is less in the latter case and, in addition to formation of spheres of reduced size, this could also lead to formation of oligomers and bridges between particles. The reduction of the percentage of hexadecane, related to the overall quantity of porogens, from the 54% to the 30% delays the phase separation and accentuates the role that the alcohol and the ketone play.

3.6 Usage of different atomizers

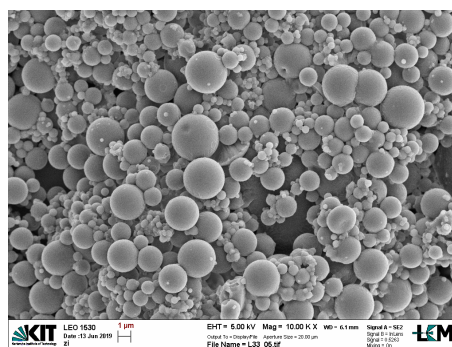
Throughout the work, two different atomizers have been used in order to evaluate the best technique for achievement of a particular particles morphology and the feasibility of the experiments, avoiding blockages of the nozzle and other side effects. Then, the aerosol generators described in Section 2.2 were employed. The second atomizer UGF 2000 by PALAS can be boosted with an extra pure nitrogen flow by another handle placed on the top of the device (Figure 2.2, under the inscription 'concentration'). The experiment L34 was performed with this extra nitrogen flow to see how it influences the process. Only solution with the most promising formulation was used in this series of experiments (Table 3.7).

Table 3.7: List of the experiments conducted with the different models of the atomizers.

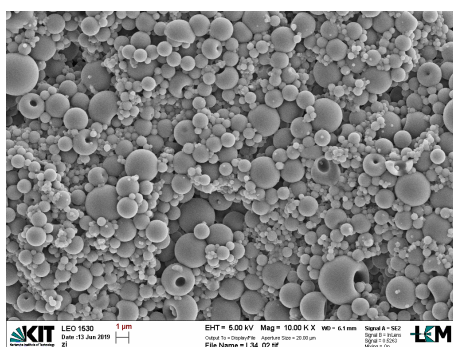
Exp.	Formulation spray solution						Reactor	Atomizer	
	Reactants		Porogens			Co-solvent			Amount
			HD	2-Oct	IsoOct				
L31	TMPMP	TMPTA	6,00	7,00	7,00	Acetone	30,00	2-tubes	ATM220
L33	TMPMP	TMPTA	6,00	7,00	7,00	Acetone	30,00	2-tubes	UGF2000
L34	TMPMP	TMPTA	6,00	7,00	7,00	Acetone	30,00	2-tubes	UGF2000 boost



(a) FE-SEM image of experiment L31.



(b) FE-SEM image of experiment L33.



(c) FE-SEM image of experiment L34.

Figure 3.12: FE-SEM images of experiments described in Table 3.7.

Each experiment of this series was conducted in the 2-tubes photoreactor, thus these results should not match the previous ones commented beforehand, although the same spray solution recipe was employed. Reasons will be explained in Section 3.7. Except for some collapsed particles, rounded and almost individual spheres were obtained for the experiment L31 (Figure 3.12a). Also in Figure 3.12b most of the particles are spherical. In the last picture more capsules can be spotted, including particles with a diameter of 1 µm.

Operative conditions in the first two compared experiments are the same even if the atomizers are different, therefore the results should be the same and actually they are. Mechanism of work of the atomizers does not affect the reaction or the condition of droplets for this solution at this operating pressure.

It runs differently for the last experiment where the residence time in the photoreactor is reduced. The extra nitrogen flow should help to have a narrow size distribution of particles, since it enhances the separation efficiency of particles bigger than 1 μm , but no differences are identified among the pictures. Perhaps, the aerosol flow should be boosted much more to identify significant differences, so more experiment varying this parameter might be conducted to confirm its effect. However, experiment L34 formed a reasonable amount of capsules. The dilution might lead to a higher rate of evaporation of the co-solvent, which helps to form capsules. Nevertheless the residence time in the photoreactor is shortened, which can also affect phase separation, cross-linking, but more experiments should be conducted to figure this effect out.

3.7 Usage of the three models of photoreactor

As anticipated before in Section 2.2, three different configuration has been experimented to assess how the reactor configurations might affect the process. The most significant parameter is tabulated below.

Table 3.8: Details of each process configuration.

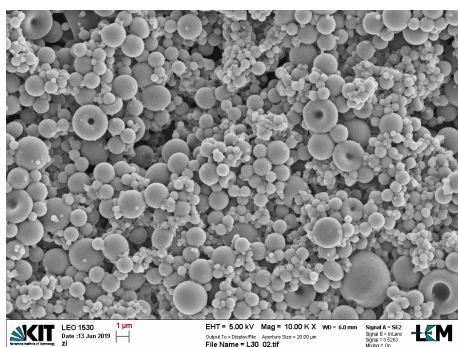
Photoreactor	Flow rate [L/s]	Residence time [s]
Quartz tube	0,0258	36,17
2-tubes	0,0162	10,86
4-tubes	0,0258	13,59

The residence time was evaluated measuring the outflow of the each reactor at the pressure of 1 bar. Only for the 2-tubes reactor, the pressure was decreased to 0.5 bar to enhance the residence time, thus to allow occurrence of the slow thiol-ene reaction. The extremely reduced available volume for the reaction combined with the high flow rate at pressure of 1 bar would have given a residence time of about 6 s, definitely too low for thiol-ene reactions. Nevertheless, proceeding in this way, the residence time is still the lowest of the series, so results based on a trend of this parameter could be outlined.

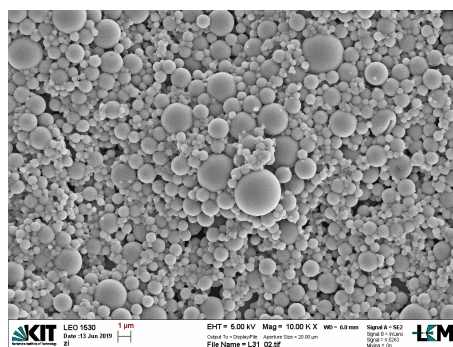
Table 3.9: List of the experiments performed in different photoreactor models.

Exp.	Formulation spray solution						Reactor	Atomizer	
	Reactants		Porogens			Co-solvent			Amount
			HD	2-Oct	IsoOct				
L30	TMPMP	TMPTA	6,00	7,00	7,00	Acetone	30,00	quartz tube	ATM220
L31	TMPMP	TMPTA	6,00	7,00	7,00	Acetone	30,00	2-tubes	ATM220
L72	TMPMP	TMPTA	6,00	7,00	7,00	Acetone	30,00	4-tubes	ATM220
L39	PETMP	TMPTA	6,00	7,00	7,00	Acetone	30,00	2-tubes	UGF2000
L87	PETMP	TMPTA	6,00	7,00	7,00	Acetone	30,00	4-tubes	ATM220
L102	PETMP	TMPTA	6,00	7,00	7,00	Acetone	30,00	quartz tube	ATM220

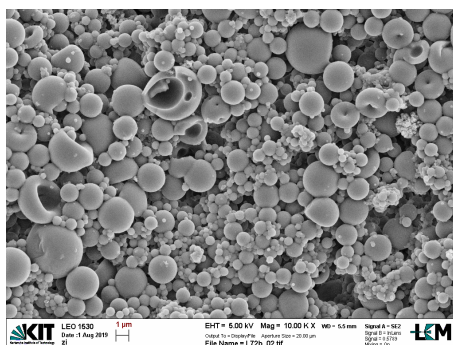
Although the same recipe to prepare the spray solution was used, the pictures below, of both series of experiments in Table 3.9, show variation in particles morphology. About the TMPMP-TMPTA combination, the lowest residence time derived from the 2-tubes reactor gave no hollow particles (Figure 3.13b). Cavities appear with the 4-tubes photoreactor, since the residence time of every single droplet is increased for at least 3 s, but they are not as defined as in Figure 3.13a where particles are characterized by smaller holes and very smooth and rounded surface. The reason is linked to the global rate of reaction that is made up of different steps such as the creation of a radical by reaction with the photoinitiator and the overall time that the polymer takes to be formed. Thus, the amount of photoinitiator that takes part into the reaction is another important parameter. The less the residence time is, the less is the amount of the reacting photoinitiator. In this way, path of the creation of longer chain is preferred, because a few radicals that start a polymeric chain can be formed. This makes polymeric matrix less cross-linked and as outlined in Section 3.2 it slows down the speed of reaction and allows to obtain either spherical particles or hollow particles with irregular shape. So considering this M/S ratio, for this combination of monomers, higher residence times are recommended.



(a) FE-SEM image of experiment L30.



(b) FE-SEM image of experiment L31.



(c) FE-SEM image of experiment L72.

Figure 3.13: FE-SEM images of experiments described in Table 3.9.

In series PETMP-TMPTA (pictures in Figure 3.14), morphology variation is not as marked as the previous one but it exists, since capsules-like particles can be spotted in Figure 3.14a. Here, number of functional groups involved within the reaction is increased, therefore propagation of the polymeric chain is faster. In fact, particles formed in the quartz tube (Figure 3.14c) look rounded and sticky, while particles formed in the 4-tubes reactor are more individual. High residence times might bring to the formation of bridges between the particles due to the high exposure to photoinitiator molecules. Perhaps, it could have happened also to the TMPMP-TMPTA combination if the residence time had been increased. PETMP-TMPTA seems to give same results of the previous monomer combination in shorter residence times.

Some capsules are located on sample taken from the experiment with the 2-tubes reactor. This experiment was conducted with the UGF 2000 atomizer at the same pressure, but with extra nitrogen flow. As observed in the previous section, experiments conducted with the boosted aerosol flow have given hollow particles regardless of the short residence time.

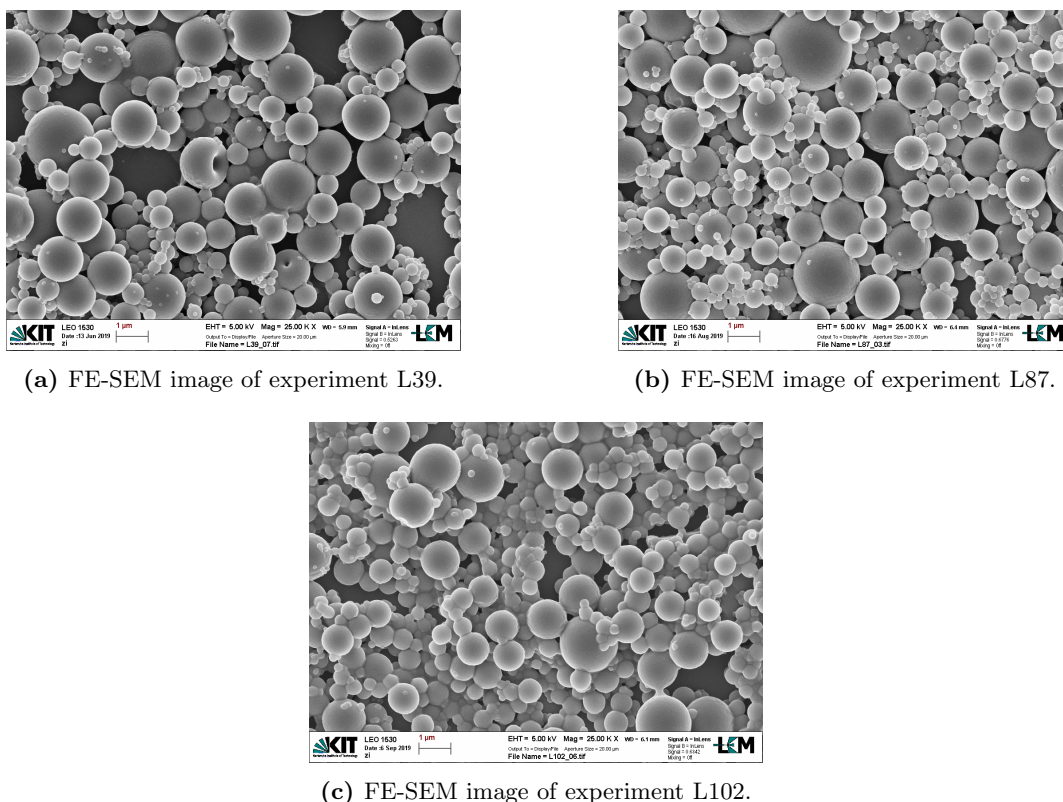


Figure 3.14: FE-SEM images of experiments described in Table 3.9.

3.8 The addition of a soft-maker: Glycerol

After several experiments involving the thiol-ene mechanism, glycerol was added to spray solution of the experiments which gave capsule-like particles. Glycerol acts as a soft-maker within the polymerization process, increasing plasticity or fluidity of a material. Polyols, in general, acts as a plasticizers. They increase void fraction of the polymer chains lowering the glass transition temperature.

Thus, this series of experiments have the purpose to verify the impact of glycerol in a thiol-ene reaction.

Table 3.10: List of experiment with glycerol and PETMP-TMPTA combination.

Exp.	Formulation spray solution							M/S Ratio	Glycerol Amount
	Reactants		Porogens			Co-solvent	Amount		
			HD	2-Oct	IsoOct				
L27	PETMP	TMPTA	8,00	3,50	3,50	EtOH	20,00	22:78	-
L89	PETMP	TMPTA	6,00	7,00	7,00	EtOH	20,00	29:71	10,00
L87	PETMP	TMPTA	6,00	7,00	7,00	Acetone	30,00	29:71	-
L88	PETMP	TMPTA	6,00	7,00	7,00	Acetone	20,00	29:71	10,00

Glycerol was added to each spray solution taking into account that volume must not exceed 80 ml (because of the flask maximum capacity). Therefore, in the experiment with acetone as a co-solvent, 10 g of acetone were replaced with 10g of glycerol. The experiment L88 gave solubility problems because of the scarce affinity between glycerol and acetone. Solubility in this co-solvent is very low (about 1g/15 ml) and phase separation took place within the flask,

nevertheless the experiment was carried out in order to make a valid comparison. Glycerol is more soluble in alcohols, instead; the solution was slightly turbid, indeed.

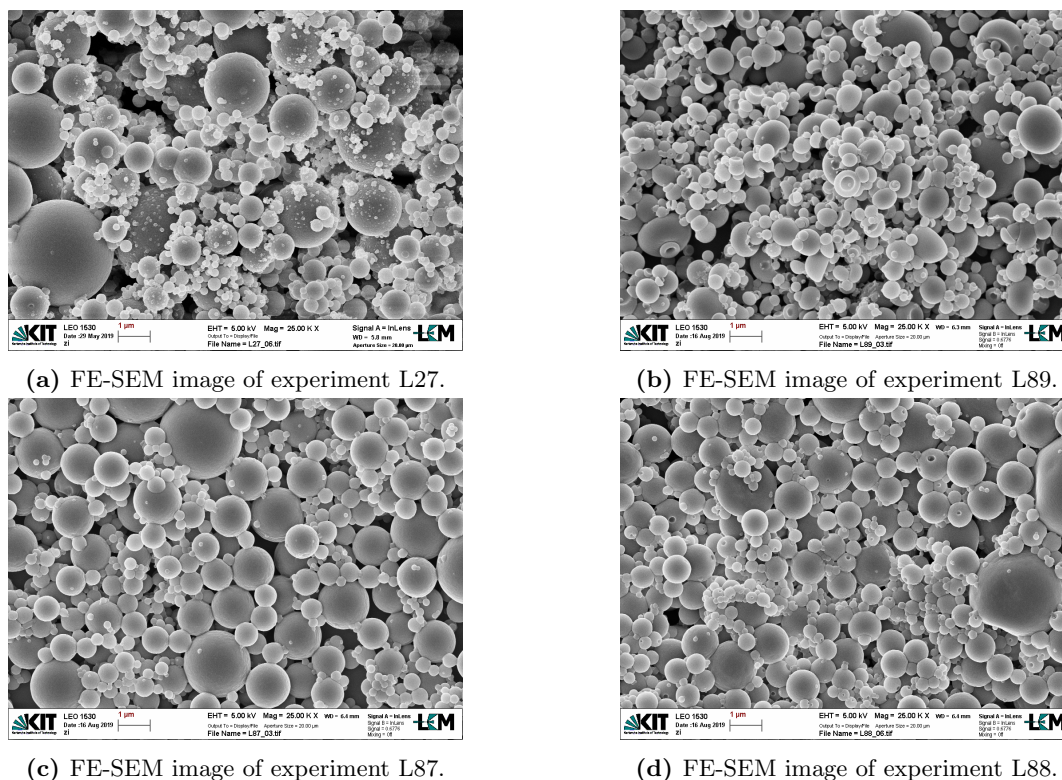


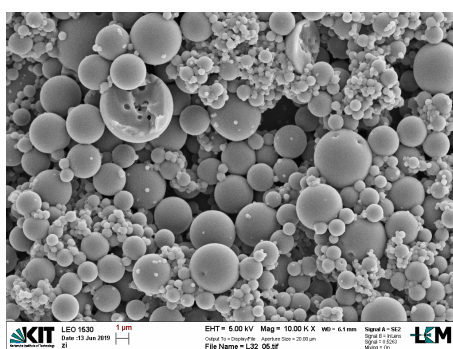
Figure 3.15: FE-SEM images of experiments described in Table 3.10.

In each experiment conducted without the addition of glycerol, particles look rounded and almost individual exclusively. In pictures 3.15b and 3.15d a great number of particles are collapsed due to the presence of glycerol. Where acetone is used as a co-solvent, particles maintained a spherical shape with spread holes around their entire surface. In contrast to what is said beforehand, nanoparticles show several cavities as well and a lot of nanocapsules were produced. Where ethanol is used, particles look much more collapsed and a great amount of nanocaps were produced. The effect of glycerol is more evident thanks to the better solubility in alcohols. Through the photoreactor, evaporation of co-solvent promotes phase separation among components that made up the droplet, in which the polymer is placed in the outer part and the core is liquid. Glycerol delays the gelation point during the co-solvent evaporation and in this way, it allows polymer to collapse in the empty core. Therefore, phase separation is a crucial step for caps formation, as it is the first step.

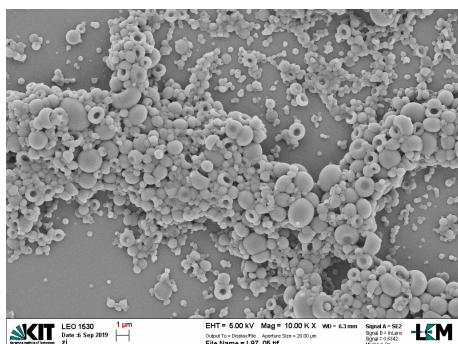
Also experiments with TMPMP-TMPTA combination were performed. Different formulation were tested. To avoid solubility problems, glycerol replaced half amount of 2-Octanone in the experiment L95 whereby acetone is used in order to keep the M/S ratio constant.

Table 3.11: List of experiment with glycerol and TMPMP-TMPTA combination.

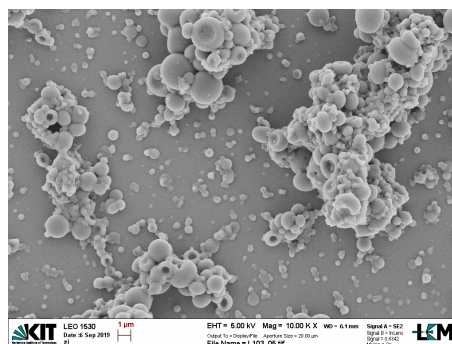
Exp.	Formulation spray solution							M/S Ratio	Glycerol Amount
	Reactants		Porogens			Co-solvent	Amount		
			HD	2-Oct	IsoOct				
L32	TMPMP	TMPTA	6,00	7,00	7,00	EtOH	30,00	29:71	-
L97	TMPMP	TMPTA	6,00	7,00	7,00	EtOH	20,00	29:71	10,00
L103	TMPMP	TMPTA	6,00	7,00	7,00	EtOH	20,00	29:71	10,00
L72	TMPMP	TMPTA	6,00	7,00	7,00	Acetone	30,00	29:71	-
L95	TMPMP	TMPTA	6,00	3,50	7,00	Acetone	30,00	29:71	3,50
L74	TMPMP	TMPTA	6,00	7,00	7,00	PrOH	30,00	29:71	-
L98	TMPMP	TMPTA	10,00	-	10,00	PrOH	20,00	29:71	10,00
L99	TMPMP	TMPTA	6,00	7,00	7,00	PrOH	10,00	29:71	10,00



(a) FE-SEM image of experiment L32.



(b) FE-SEM image of experiment L97.



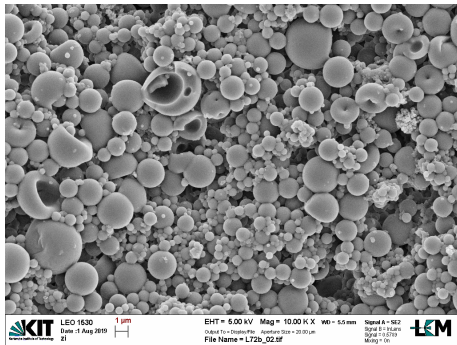
(c) FE-SEM image of experiment L103.

Figure 3.16: FE-SEM images of experiments described in Table 3.11.

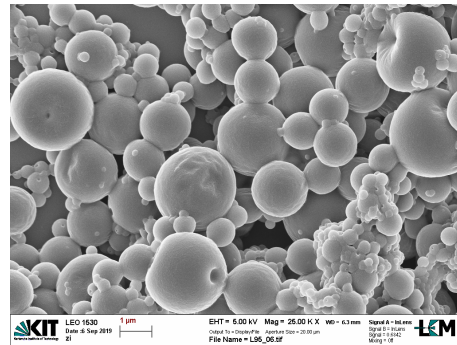
Also with this monomer combination nanocaps were produced. Glycerol proved to be fundamental for production of nanocaps by thiol-ene polymerization, since none of the previous experiments gave same results. In the experiment L32, shown in Figure 3.16a, only bigger particles are mildly collapsed. This is due to the fact that the polymer matrix is not that flexible like when glycerol is used and the free volume generated from evaporation of ethanol produces pores and narrow cavities within the particle. During phase separation, volume occupied by the co-solvent is not enough to promote collapse of the outer part of the particle, made up of polymer. The broken particle in the figure allows to claim that this spray solution formulation does not lead to neither capsules formation nor hollowed nanoparticles.

Experiments L97 and L103 were conducted with the same spray formulation but the former used the 4-tubes photoreactor and the latter the quartz tube one. What has been told for the PETMP-TMPTA monomer combination is valid in this case as well. Nanocaps were produced

thanks to the enhancement of flexibility and swellability of the formed material. It is possible to confirm what has been told about the photoreactor differences in Section 3.7; the experiment L103 shows less individual nanocaps with presence of bridges between particles, probably, because of an higher residence time.



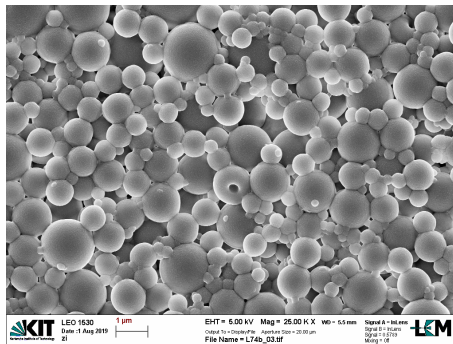
(a) FE-SEM image of experiment L72.



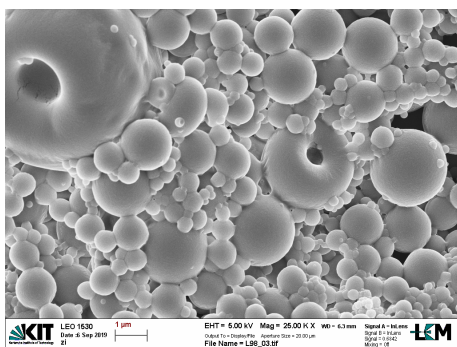
(b) FE-SEM image of experiment L95.

Figure 3.17: FE-SEM images of experiments described in Table 3.11.

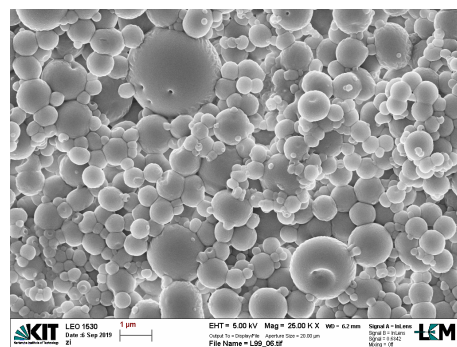
Using acetone as a co-solvent, is not possible to see the effect of glycerol, instead. Capsules were produced because of high volatility of co-solvent (Figure 3.17a that generates greater volumes than ethanol can do, during evaporation). Despite the reduced amount of glycerol, spray solution still remained turbid and phase separation took place within the flask, with all the soft-maker placed on bottom of the flask. 2-Octanone also helps to keep solutions homogenous acting as a good solvent. Therefore, in presence of acetone results are not reliable and path without glycerol is preferred.



(a) FE-SEM image of experiment L74.



(b) FE-SEM image of experiment L98.



(c) FE-SEM image of experiment L99.

Figure 3.18: FE-SEM images of experiments described in Table 3.11.

Experiments with n-propanol were also performed. The already discussed results for the experiment L74 outlined that collapse of particles with this co-solvent is very rare. The addition of glycerol brought no significant improvements on the particles morphology. In fact, collapsed particles are still a few in Figure 3.18b and even less in Figure 3.18c. Glycerol was well solubilised in the mixture, so surely it was contained in sprayed droplets. Nonetheless, the decreasing of co-solvent vapor pressure worsened the creation of a void space within the particle and polymer could not collapse even though its swellability increased (particles look oval and irregular). Moreover, in the experiment L98 phase separation was enhanced by the high amount of hexadecane, pushing homogeneity of the spray solution to the limit. This enhancement could be the responsible of an higher number of capsules formed. However, the high amount of 2-ethylhexanol could have increased the stickiness of the polymer, as shown in Section 3.5.

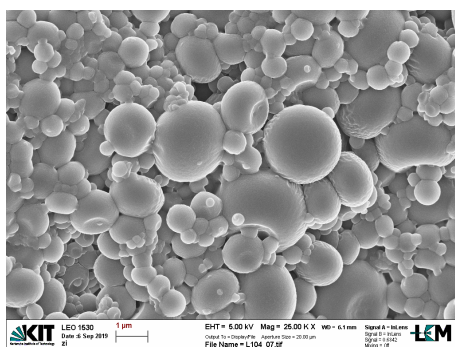
Below, combination TMPMP-BVE was experimented. Based on previous results, no experiments with glycerol and acetone were conducted. But unfortunately, there are no experiments in presence of only ethanol as a co-solvent and M/S ratio was not kept constant because since from the first experiment made, this combination did not show as interesting as the others.

Table 3.12: List of experiments with glycerol and TMPMP-BVE combination.

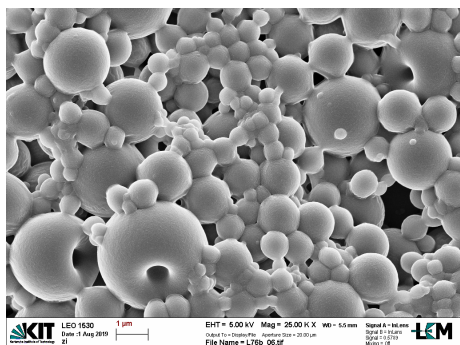
Exp.	Formulation spray solution							M/S Ratio	Glycerol Amount
	Reactants		Porogens			Co-solvent	Amount		
			HD	2-Oct	IsoOct				
L104	TMPMP	BVE	6,00	7,00	7,00	EtOH	20,00	29:71	10,00
L76	TMPMP	BVE	8,00	3,50	3,50	Acetone	20,00	36:64	-
L81	TMPMP	BVE	8,00	3,50	3,50	Acetone	20,00	22:78	-

In fact, in Figure 3.19b, only a few big capsules are produced. Particles look very sticky and sometimes even merged. Analysing the experiment L81, in which M/S is decreased, no hollow particles are formed and they are almost spherical and individual. With the decreasing of M/S, polymerization is slower and phase separation within the droplet worsens. Also the decreasing of number of functional groups involved in polymerization lower reaction speed.

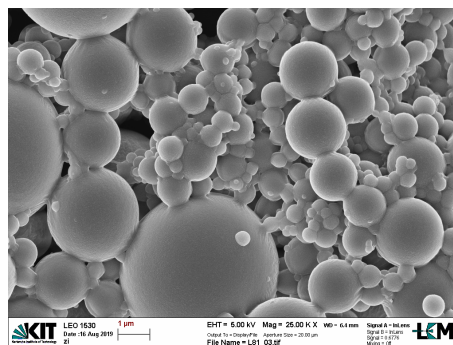
Considering this aspects, only an experiment with ethanol and glycerol was performed and result is shown in Figure 3.19a. As in experiments L98 and L99, particles have an oval shape that claims that glycerol acted as a soft-maker, but no capsules or caps can be spotted. For this reason, this combination was actually rejected.



(a) FE-SEM image of experiment L104.



(b) FE-SEM image of experiment L76.



(c) FE-SEM image of experiment L81.

Figure 3.19: FE-SEM images of experiments described in Table 3.12.

3.9 Incorporation of silver nanoparticles

Aerosol-photopolymerization technique was also investigated for generation of hybrid particles. Aim of the experiments performed was to incorporate silver nanoparticles *in situ* into capsules-like particles formed by the thiol-ene mechanism. The best formulations of the spray solutions were reproduced with addition of different mixtures containing silver nanoparticles. In this case, once that the spray solution was ready, it was stirred for at least 24 hours to allow particles to be totally dispersed within the solution. Analysis by SEM and TEM are shown below.

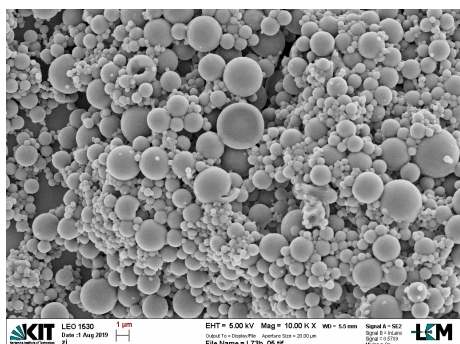
Table 3.13: List of experiments with addition of silver nanoparticles.

Exp.	Formulation spray solution						M/S Ratio	Glycerol Amount	Silver solution Amount	
	Reactants		Porogens		Co-solvent	Amount				
			HD	2-Oct	IsoOct					
L73	TMPMP	TMPTA	6,00	7,00	7,00	Acetone	30,00	26:74	-	6,00
L100	TMPMP	TMPTA	6,00	7,00	7,00	PrOH	20,00	25:75	10,00	10,00
L105	TMPMP	TMPTA	6,00	7,00	7,00	EtOH	20,00	25:75	10,00	10,00

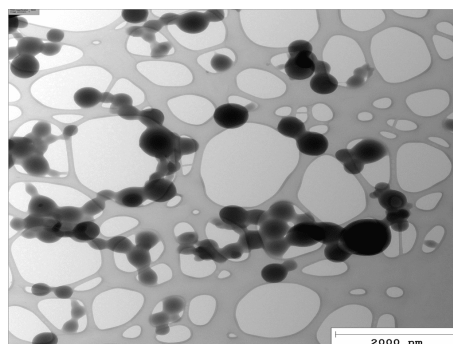
The experiments that formed microcapsules and nanocaps were reproduced as mentioned before in the previous subsections. Silver ink was used in the experiment L73 and the silver nanodispersion was used in the experiments L100 and L105. Nevertheless, SEM pictures below show anything but sponges and sticky irregular particles. For this reason also TEM images show that incorporation of such nanoparticles was failed and furthermore, where glycerol is employed, silver formed agglomerates of 2 µm of size placed outside the polymeric matrix.

The propagation step of this mechanism might occur in parallel with reaction between thiyl radicals and silver particles, thus propagation step is hindered. Since also Irgacure 907 tends to

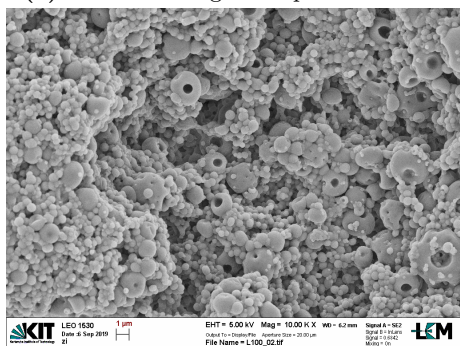
react with silver ions, the original amount of photoinitiator was doubled from 1% of the overall monomer to 2% , in the last two experiments of the series, to overcome its parallel consumption. However, no improvements were observed. Detailed studies on the kinetics of the process and evaluation of the entity of this parallel phenomena might help to understand which are main causes of the failure.



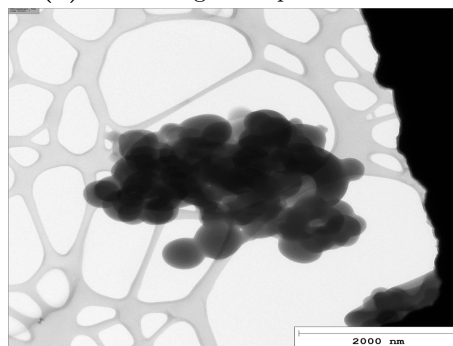
(a) FE-SEM image of experiment L73.



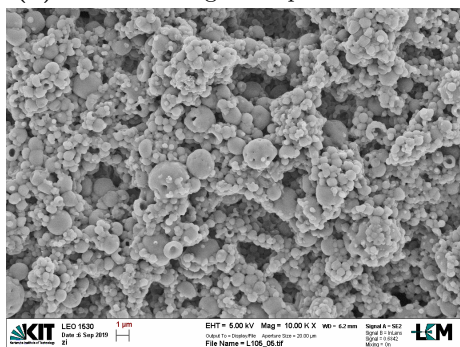
(d) TEM image of experiment L73.



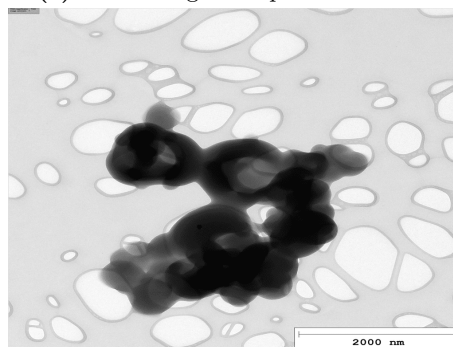
(b) FE-SEM image of experiment L100.



(e) TEM image of experiment L100.



(c) FE-SEM image of experiment L105.



(f) TEM image of experiment 105.

Figure 3.20: FE-SEM and TEM images of experiments shown in Table 3.13.

Chapter 4

Results and discussion: Chain polymerization

Experiments about acrylic radical polymerization were carried out as well. As was done in the previous chapter, the procedure starts to analyse different acrylic monomers in order to evaluate intrinsic properties of polymerization and then effect of modification of the spray formulation were analysed. Every experiment was performed with 10 g of monomer and the 4-tubes photoreactor was used.

4.1 Morphology of acrylic polymer particles

Four different monomers were employed for each series of experiment, in particular:

- Trimethylolpropane triacrylate (TMPTA)
- Neopentyl glycol diacrylate (Neopentyl)
- 1,6-hexanediol diacrylate (HDDA)
- Trimethylolpropane ethoxylate triacrylate (TMPe7TA)

Given that an homopolymerization mechanism occurs, 4 different experiments were conducted for each spray solution formulation. In Table 4.1 experiments without addition of a co-solvent are shown.

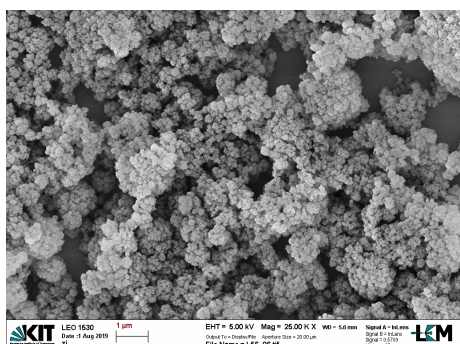
Table 4.1: List of experiments with acrylic monomers without using a co-solvent.

Exp.	Formulation spray solution					M/S Ratio	Functional groups	
	Monomer	Porogens			Co-solvent			Amount
		HD	2-Oct	IsoOct				
L56	TMPTA	10,00	-	15,00	-	-	29:71	3
L59	HDDA	10,00	-	15,00	-	-	29:71	2
L60	TMPe7TA	10,00	-	25,00	-	-	22:78	3
L61	Neopentyl	10,00	-	15,00	-	-	29:71	2

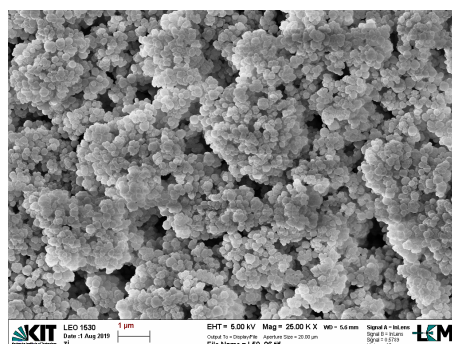
In contrast to thiol monomers, no frequent solubility problems arouse with acrylic monomers. Experiments without the addition of a co-solvent could be conducted, with the exception of TMPe7TA, which solution required 25g of Isooctanol to be homogeneous. Nonetheless, no material was collected from PTFE membrane, because of the low M/S ratio and the high quantity of isooctanol that vanishes the available monomer in the photoreactor. Therefore, amounts of

porogens were chosen to enable each experiment to perform in absence of problems of all sorts (solubility, setup malfunctions, etc.).

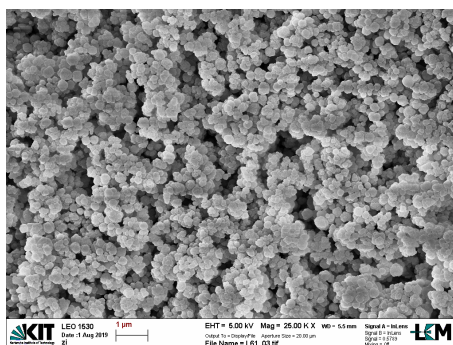
In the following pictures, polymer structure is highly detailed but particles are not always distinguishable. In fact, only in Figure 4.1a, original shape of rounded particles was kept with this characteristic modified surface. All protuberances, namely domains, that compose the outer part of particles contribute sharply to increase surface area and feature this fully shrivelled and blistry structure which resembles that of a cauliflower (mosaic structure). Observing other picture below, particles original shape is impossible to be identified. Polymer structure is partially disrupted in Figure 4.1b and entirely disrupted in Figure 4.1c. These results were further investigated with addition of ethanol, acetone and 1-propanol as co-solvents in spray solution.



(a) FE-SEM image of experiment L56.



(b) FE-SEM image of experiment L59.

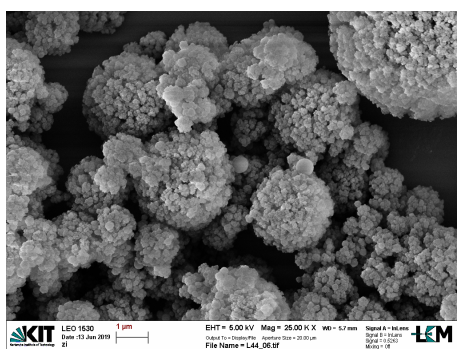


(c) FE-SEM image of experiment L61.

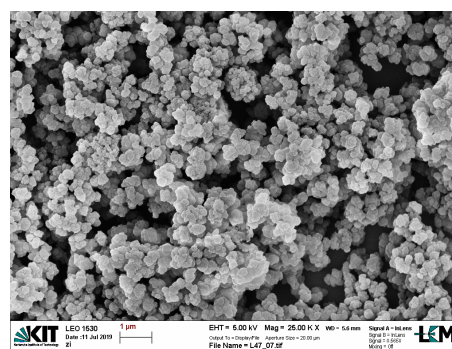
Figure 4.1: FE-SEM images of experiments described in Table 4.1.

Table 4.2: List of the experiments conducted with acrylic monomers in different co-solvents.

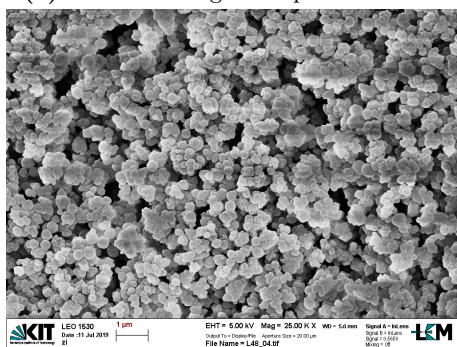
Exp.	Formulation spray solution					M/S Ratio	Functional groups	
	Monomer	Porogens			Co-solvent			Amount
		HD	2-Oct	IsoOct				
L44	TMPTA	10,00	-	10,00	EtOH	20,00	20:80	3
L47	Neopentyl	10,00	-	10,00	EtOH	20,00	20:80	2
L48	HDDA	10,00	-	10,00	EtOH	20,00	29:80	2
L49	PETA	10,00	-	10,00	EtOH	20,00	20:80	4
L50	TMPTA	10,00	-	10,00	PrOH	20,00	20:80	3
L64	HDDA	10,00	-	10,00	PrOH	20,00	20:80	2
L68	Neopentyl	10,00	-	10,00	PrOH	20,00	20:80	2
L69	TMPe7TA	10,00	-	10,00	PrOH	20,00	20:80	3
L45	TMPTA	10,00	-	10,00	Acetone	20,00	20:80	3
L62	Neopentyl	10,00	-	10,00	Acetone	20,00	20:80	2
L63	PETA	10,00	-	10,00	Acetone	20,00	20:80	4
L90	HDDA	10,00	-	10,00	Acetone	20,00	20:80	2



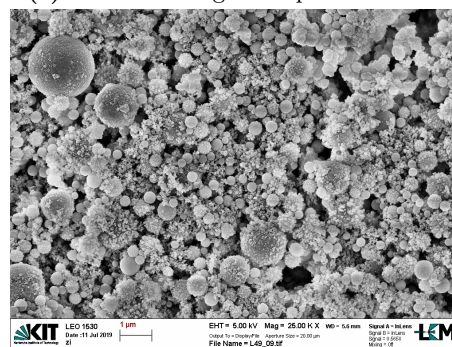
(a) FE-SEM image of experiment L44.



(c) FE-SEM image of experiment L47.



(b) FE-SEM image of experiment L48.



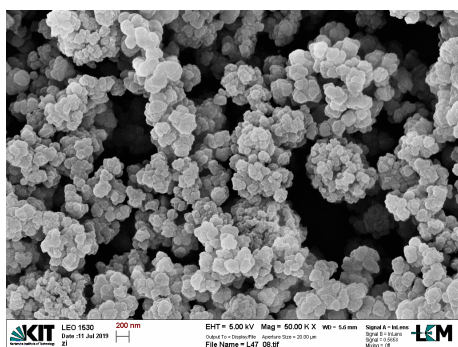
(d) FE-SEM image of experiment L49.

Figure 4.2: FE-SEM images of experiments in Table 4.2 with ethanol as co-solvent.

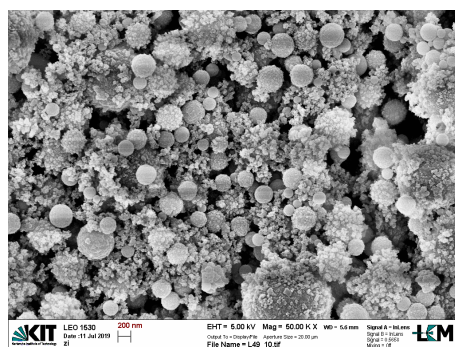
Experiments with tetrafunctionalized PETA acrylic monomer were added to the series. With addition of a co-solvent, M/S ratio is decreased and particles have almost kept their features, considering experiments shown in Figure 4.1. Volume fraction of created voids has slightly increased due to the presence of an high volatile substance. Same results are shown in the following pictures where other co-solvents are employed.

Regarding to PETA experiment (Figure 4.2d), it produced spherical micro and nanoparticles covered with a characteristic polymer decoration of tiny fragments with a dimension around 20-50 nm. Particle size distribution is very broad. In fact, particles bigger than 1 μm and smaller than 200 nm can be spotted in figures below, in which result of experiments L47 and

L49 are shown with higher magnification (50000x). Also dimension of nanodomains obtained from polymerization of Neopentyl is depicted in Figure 4.3a.

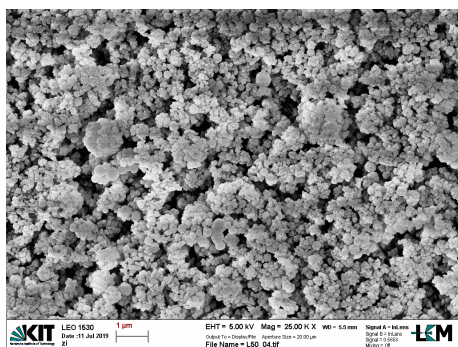


(a) FE-SEM image of experiment L47.

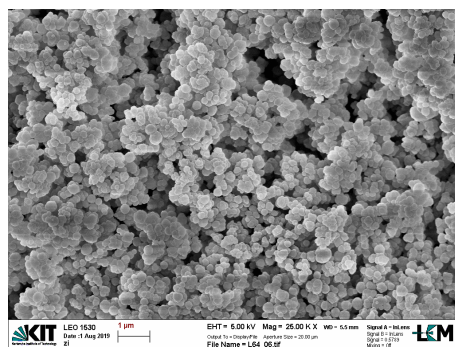


(b) FE-SEM image of experiment L49.

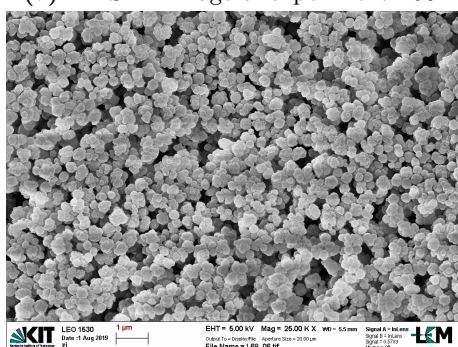
Figure 4.3: FE-SEM images of experiments in Table 4.2 with a higher magnification.



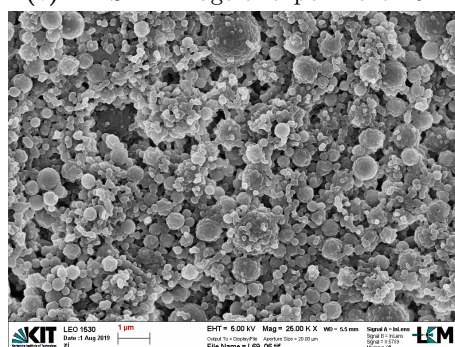
(a) FE-SEM image of experiment L50.



(c) FE-SEM image of experiment L64.



(b) FE-SEM image of experiment L68.



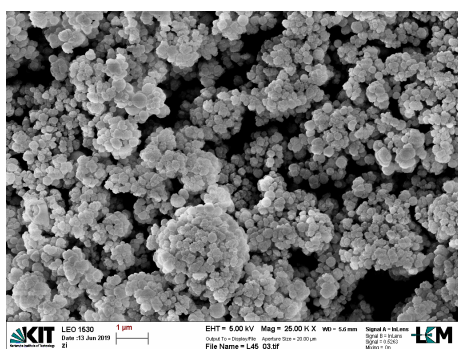
(d) FE-SEM image of experiment L69.

Figure 4.4: FE-SEM images of experiments in Table 4.2 with 1-propanol as co-solvent.

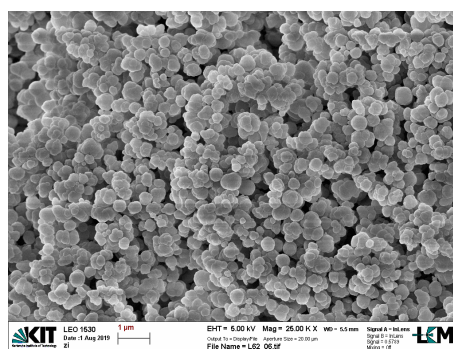
In Figures 4.4 and 4.5 same results as the previous one obtained with ethanol are shown. The three different solvent slightly modify particles morphology, keeping always the original intrinsic features of monomeric species involved. In particular, TMPe7TA was used in the 1-propanol series, showing a blistery and non-individual polymeric structure.

Morphology and polymeric structure vary in parallel with number functional groups. Actually, no significant differences might be outlined between HDDA and Neopentyl, which both have 2 functional groups. Polymer matrix is always featured with a disintegrated (or partially disintegrated) structure composed by individual nanodomains. In experiments with TMPe7TA and PETA, particles are visible even though their morphology is modified by far. Number of functional groups are strictly related to the overall speed rate of polymerization. Creation of a primary monomer radical and propagation step of the reaction depend on number of active

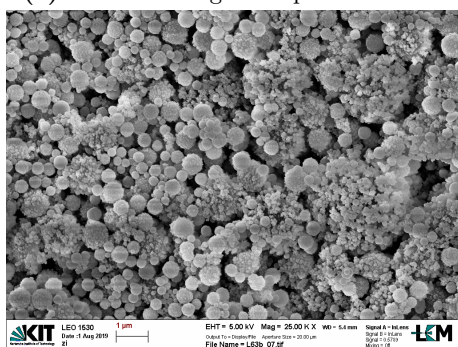
sites, namely the number of acrylic functional groups. Throughout polymeric chain growth, a linear radical molecule like HDDA and Neopentyl, placed at the end of the chain, has one available active site for another monomer attachment. Trifunctionalized and tetrafunctionalized monomers have more than one available active site, which allow polymeric chain grow with different spatial conformation, thus speed rate polymerization and polymer cross-linking increase. This phenomenon led to formation of compact structures more or less detailed on the surface. It is also strictly connected to size of particles formed. In fact, particles diameter decreases with the increasing of number of functional groups involved. PETA, which polymerization is faster than TMPTA, especially forms corrugated and decorated rounded particles, in spite of the high amount of porogens and the low M/S ratio. Therefore, number of functional groups and speed rate polymerization reveal fundamental to control morphology of particles.



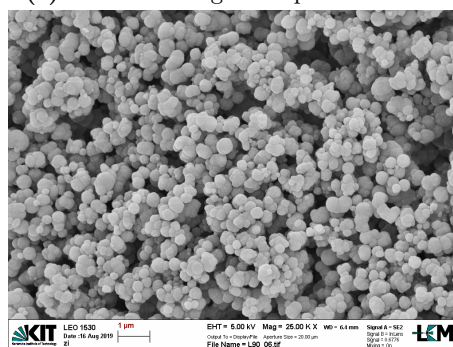
(a) FE-SEM image of experiment L45.



(c) FE-SEM image of experiment L62.



(b) FE-SEM image of experiment L63.



(d) FE-SEM image of experiment L90.

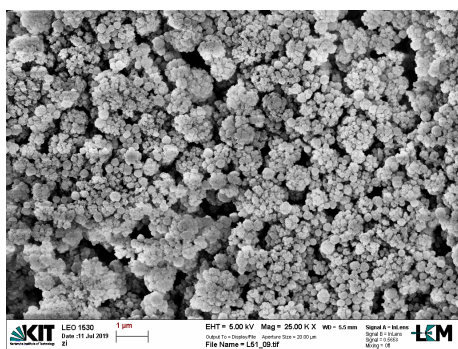
Figure 4.5: FE-SEM images of experiments in Table 4.2 with acetone as co-solvent.

4.2 Effect of porogens: Hexadecane

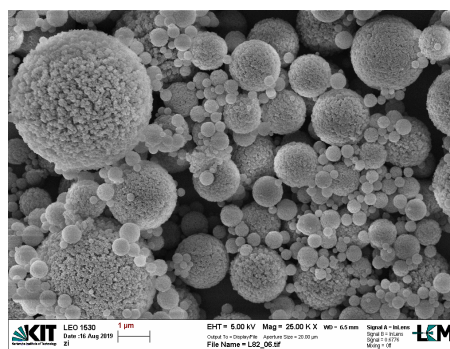
In this section and in the following one, formulations of spray solution and comparisons between experiments were established based on solubility limits and ranges of monomers. For hexadecane variations, experiments are compared below. M/P ratio was added to compare monomers amount with overall amount of porogens.

Table 4.3: List of experiments with variation of hexadecane.

Exp.	Formulation spray solution						M/S Ratio	M/P Ratio
	Monomer	Porogens			Co-solvent	Amount		
		HD	2-Oct	IsoOct				
L51	TMPTA	10,00	-	10,00	-	-	33:67	33:67
L82	TMPTA	-	-	10,00	-	-	50:50	50:50
L66	HDDA	10,00	-	-	PrOH	20,00	25:75	50:50
L67	HDDA	20,00	-	-	PrOH	20,00	20:80	33:67
L70	HDDA	-	-	-	PrOH	20,00	33:67	-



(a) FE-SEM image of experiment L51.

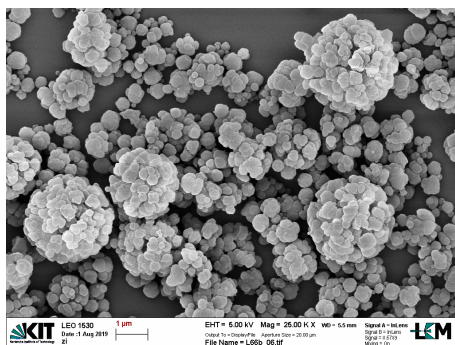


(b) FE-SEM image of experiment L82.

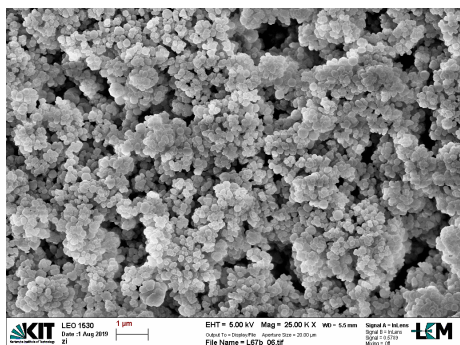
Figure 4.6: FE-SEM images of experiments in Table 4.3.

As this is a bad solvent, a few experiments could be performed in order to identify its influence. With TMPTA, microparticles with nanostructured domains were obtained in Figure 4.6b, whilst a similar polymer structure with a more detailed surface and an average particle size lower than 1 μm were obtained adding 10 g of hexadecane, in Figure 4.6a.

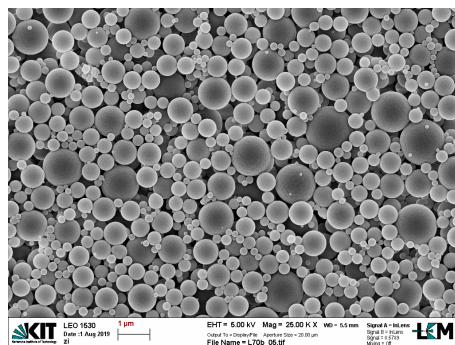
In HDDA series, with the increasing of amount of hexadecane, polymer structure showed more disintegrated, going from production of spherical and mainly smooth particles in Figure 4.7c and through production of less structured cauliflower-like particles (compared to the ones obtained with TMPTA beforehand) shown in Figure 4.7a.



(a) FE-SEM image of experiment L66.



(b) FE-SEM image of experiment L67.



(c) FE-SEM image of experiment L70.

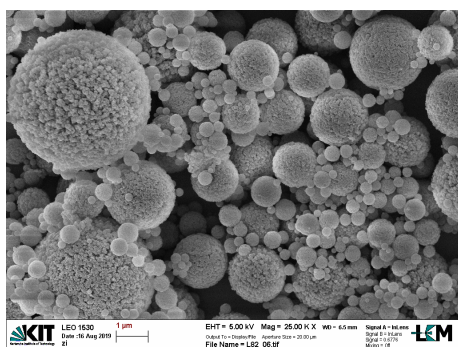
Figure 4.7: FE-SEM images of experiments in Table 4.3.

4.3 Effect of porogens: Isooctanol

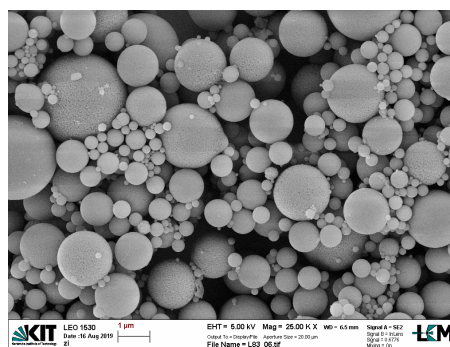
Although isooctanol is a better solvent, solubility problems arise with some monomer that forced to proceed as shown in Table 4.4. Amount of TMPTA was varied in order to prepare solution with a fixed M/S ratio.

Table 4.4: List of experiments with variation of isooctanol.

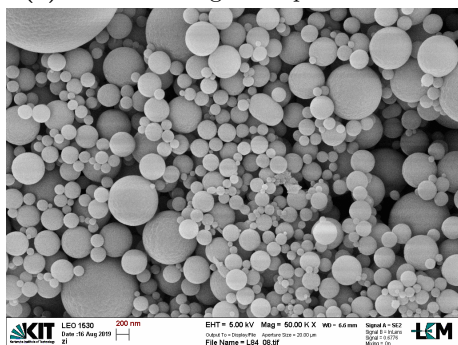
Exp.	Formulation spray solution					M/S Ratio	M/P Ratio	
	Monomer	Porogens			Co-solvent			Amount
		HD	2-Oct	IsoOct				
L82	TMPTA	-	-	10,00	-	-	50:50	50:50
L83	TMPTA	-	-	7,50	-	-	67:33	67:33
L84	TMPTA	-	-	5,00	-	-	80:20	80:20
L85	TMPTA	-	-	4,00	-	-	87:13	87:13
L86	TMPTA	-	-	-	PrOH	20,00	33:67	-
L64	HDDA	10,00	-	10,00	PrOH	20,00	20:80	33:67
L66	HDDA	10,00	-	-	PrOH	20,00	25:75	50:50
L71	HDDA	10,00	-	20,00	PrOH	20,00	17:83	25:75



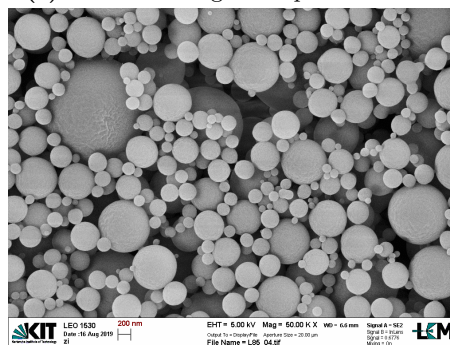
(a) FE-SEM image of experiment L82.



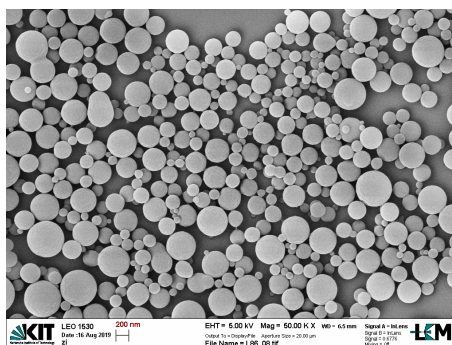
(c) FE-SEM image of experiment L83.



(b) FE-SEM image of experiment L84.



(d) FE-SEM image of experiment L85.

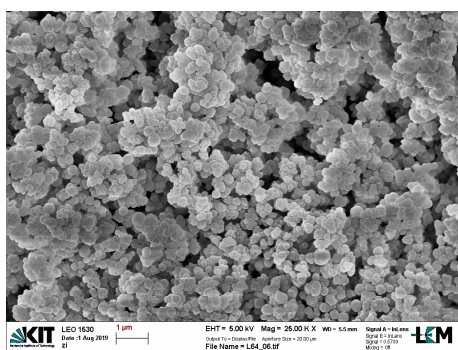


(e) FE-SEM image of experiment L86.

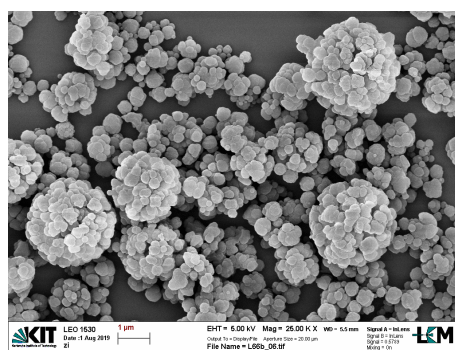
Figure 4.8: FE-SEM images of TMPTA series of experiments shown in Table 4.4.

In this case, amount of isooctanol was lowered through TMPTA series. Observing the 5 pictures of Figure 4.8 from the first to the last, particles turn smoother and less structured until chill-type particles were obtained with the only addition of 1-propanol. Particle size distribution became narrower with a peak shifted to sizes in the nanometric range. In the series, the first two pictures are obtained with the common magnification of 25000x, while the other magnification was doubled in order to evaluate the differences.

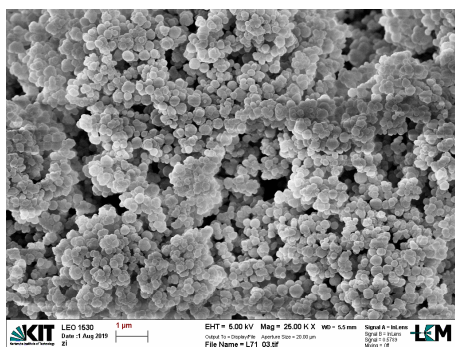
As a high volatile compound, role of co-solvent has been already discussed beforehand. For experiments without co-solvent, instead, monomers might polymerize faster when there are less molecules that do not take part in reaction. A reduced amount of porogens might enhance efficiency of polymerization, thus cross-linking and smaller size are preferred as well, to the detriment of high structured surfaces. Effects on speed polymerization rate, here are more evident, because of lower amount of porogens. M/S ratio favours monomer, so a slight increase of this parameter when value is above 70:30, might strongly affect the chain polymerization mechanism. When M/S ratio 50:50 or less, variation of porogens quantity is not so decisive, since they still occupy most of the droplet volume throughout the photoreactor passage.



(a) FE-SEM image of experiment L64.



(b) FE-SEM image of experiment L66.



(c) FE-SEM image of experiment L71.

Figure 4.9: FE-SEM images of HDDA series of experiments in Table 4.4.

In presence of a co-solvent, as occurred for HDDA series, M/S ratio does not match with M/P ratio and consideration without a co-solvent contribute can be drawn. What is valid for TMPTA is valid also for HDDA if M/P ratio is taken into account. A high M/P ratio favours speed rate of polymerization and allows polymer to create a detailed structure that reminds that of a cauliflower (Figure 4.9b). Disruption of polymer matrix increased as M/P ratio decreased, since porogens role prevailed.

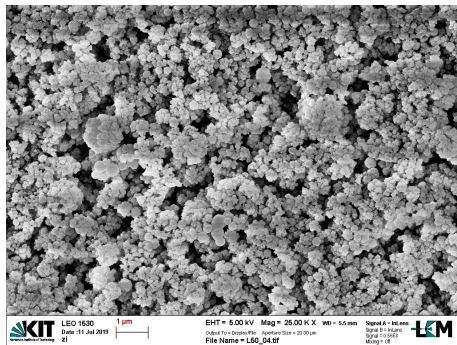
Thus, regardless of presence of a co-solvent in spray solution, M/P ratio establishes particles morphology of each monomer employed. Below, some experiment, in which M/P is kept constant are compared.

Table 4.5: List of experiments with same M/P ratio.

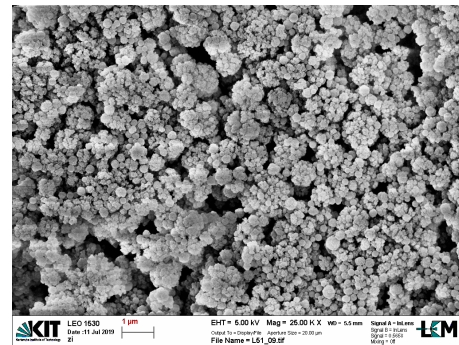
Exp.	Formulation spray solution						M/S Ratio	M/P Ratio
	Monomer	Porogens			Co-solvent	Amount		
		HD	2-Oct	IsoOct				
L50	TMPTA	10,00	-	10,00	PrOH	20,00	20:80	33:67
L51	TMPTA	10,00	-	10,00	-	-	33:67	33:67
L57	HDDA	10,00	-	10,00	-	-	33:67	33:67
L64	HDDA	10,00	-	10,00	PrOH	20,00	20:80	33:67

TMPTA kept same mosaic cauliflower structure in Figures 4.10a and 4.10c even though average particle size slightly varied because of presence of a co-solvent. For HDDA series instead, a partial disrupted structure is conserved. Presence of a co-solvent is crucial to keep the spray

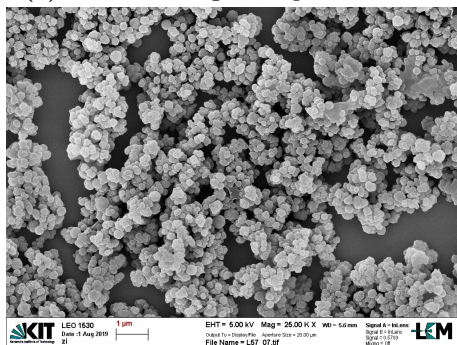
solution homogeneous and to create several combinations of spray formulation that allows to attain different morphologies, but it does not affect surface features of particles. The roles of hexadecane and isooctanol differs from each other within the entire process and they might be more or less evident proportionally to amount of this porogens added to spray solution. Therefore, keeping the same M/P ratio, results from an experiment with only hexadecane as porogen might differ from those of an experiment in which only isooctanol is employed. However, differences are not that consistent.



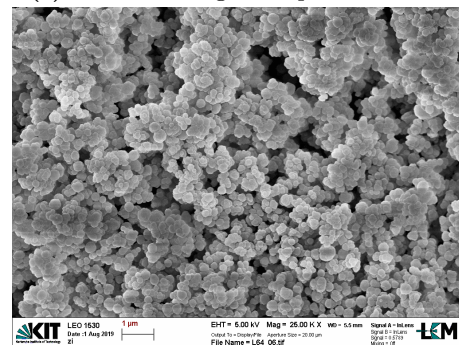
(a) FE-SEM image of experiment L50.



(c) FE-SEM image of experiment L51.



(b) FE-SEM image of experiment L57.



(d) FE-SEM image of experiment L64.

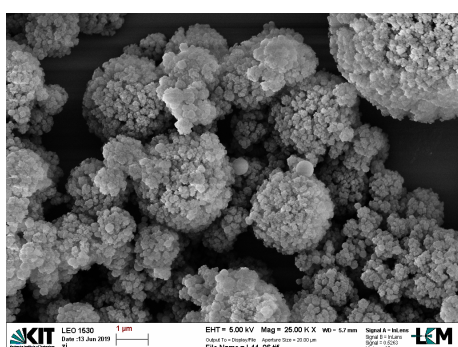
Figure 4.10: FE-SEM images of TMPTA series of experiments in Table 4.4.

4.4 Effect of porogens: 2-Octanone

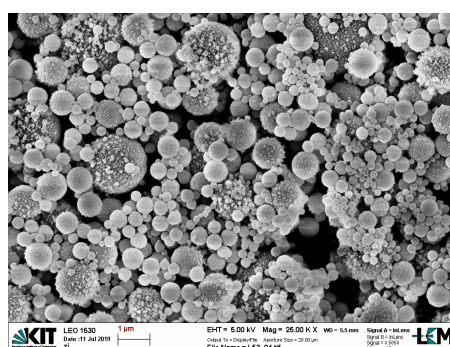
Only an attempt with the aim of replacing isoctanol with 2-octanone was made in the entire work. Given that acrylic monomer often do not show solubility problems, it is not necessarily required as with thiol-ene monomers.

Table 4.6: List of experiments with variation of 2-octanone.

Exp.	Formulation spray solution						M/S Ratio	M/P Ratio
	Monomer	Porogens			Co-solvent	Amount		
		HD	2-Oct	IsoOct				
L44	TMPTA	10,00	-	10,00	EtOH	20,00	20:80	33:67
L53	TMPTA	10,00	10,00	-	EtOH	20,00	20:80	33:67



(a) FE-SEM image of experiment L44.



(b) FE-SEM image of experiment L53.

Figure 4.11: FE-SEM images of experiments in Table 4.6.

A broad size distribution of particles was obtained from experiment L53. However, the distribution shifted to lower size values. A light decoration of small nanodomains appeared to the detriment of the well detailed structure of experiment L44, especially on particles bigger than 1 μm . 2-octanone is a good solvent and it delays polymer gelation and also phase separation within the droplet, due to the better solubility of the substances employed. The better the homogeneity in the spray solution is, the less the surface structure of the particles is shrivelled and blistered. This is also shown in the series of TMPTA in Figure 4.8 in which the homogeneity rate decreases with the reduction of isoctanol in the spray mixture. So phase separation is a fundamental step to determine morphology of particles and its delay lead to a chill-type structure.

4.5 Incorporation of silver nanoparticles

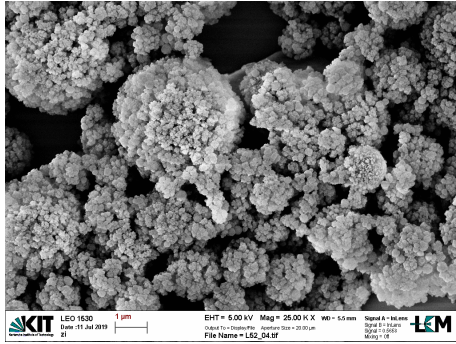
Generation of hybrid particles was also investigated for acrylic polymerization. As with thiol-ene polymerization, the spray solution was stirred for at least 24 hours before mounting the flask into the atomizer.

Table 4.7: List of experiments with addition of silver nanoparticles.

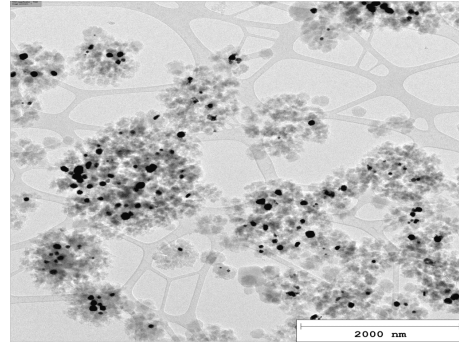
Exp.	Formulation spray solution						M/P Ratio	Silver particles	
	Monomer	Porogens		Co-solvent	Amount	Type		Amount	
		HD	2-Oct	IsoOct					
L52	TMPTA	10,00	-	10,00	PrOH	20,00	33:67	ink	6,00
L75	TMPTA	10,00	-	10,00	PrOH	20,00	33:67	nano-dispersion	3,00
L77	TMPTA	10,00	-	10,00	PrOH	20,00	33:67	AgBF ₄	0,902
L101	TMPTA	-	-	15,00	-	-	40:60	nano-dispersion	10,00
L93	HDDA	10,00	-	5,00	-	-	40:60	nano-dispersion	10,00
L94	HDDA	10,00	-	5,00	-	-	40:60	AgBF ₄	0,902

Particles with nanostructured surface were employed for the incorporation of silver nanoparticles. The spray solution with TMPTA and the best M/P ratio was reproduced and different mixtures containing the silver nanoparticles were tried. As can be seen in the SEM pictures below, morphology of the particles shown kept always the same structure except for experiment L77 in Figure 4.12c, in which a slight decoration appeared on the particles surface.

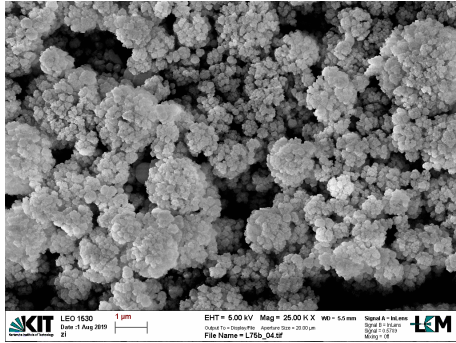
Excluding experiment L77, silver nanoparticles were well dispersed into the spray solution and the outcomes of the tests were positive. The cauliflower structure is preserved and incorporation of silver nanoparticles was quite successful for both the silver nano-dispersion and the silver ink. TEM pictures depicted a collection of black spots (of about 50 nm) spread inside each polymeric particle, from the biggest one to the smallest. In experiment L101, the original amount of photoinitiator was doubled to overcome its consumption due to the parallel reaction with silver and results were positive, nonetheless. The spray solution with AgBF₄ did not stay homogeneous throughout the experiment and a layer of non-dissolved substances laid on the bottom of the flask. Silver salt might be highly reactive and more sensible to the presence of the photoinitiator, therefore it is not suitable for this process.



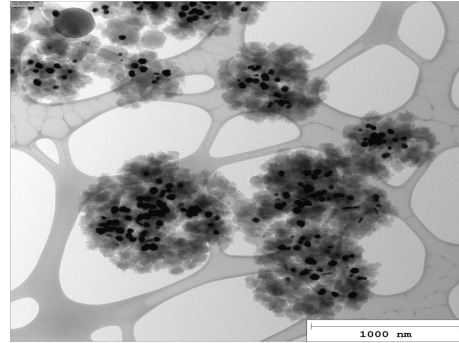
(a) FE-SEM image of experiment L52.



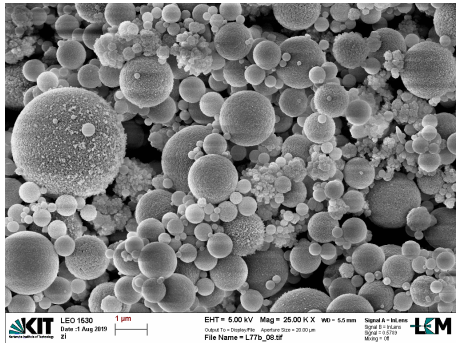
(e) TEM image of experiment L52.



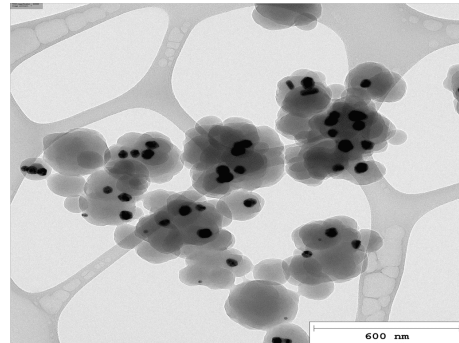
(b) FE-SEM image of experiment L75.



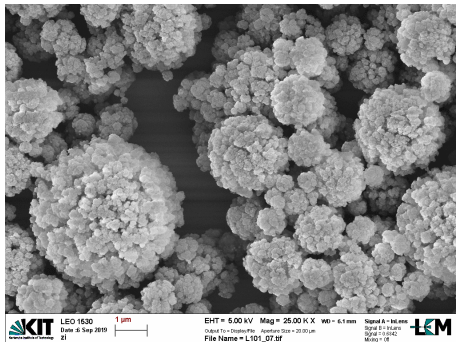
(f) TEM image of experiment L75.



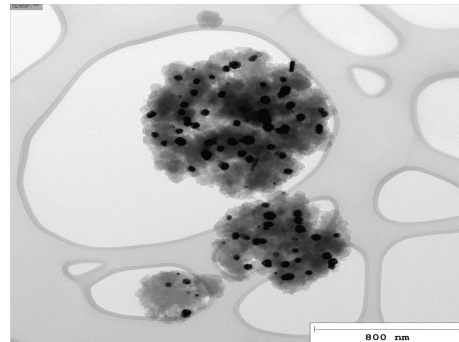
(c) FE-SEM image of experiment L77.



(g) TEM image of experiment L77.

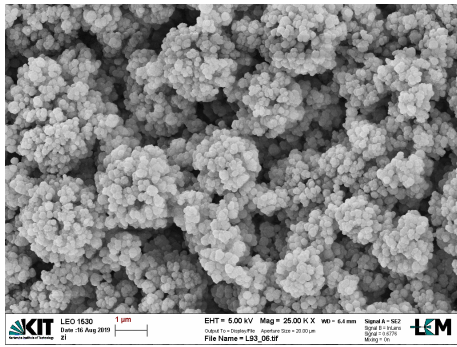


(d) FE-SEM image of experiment L101.

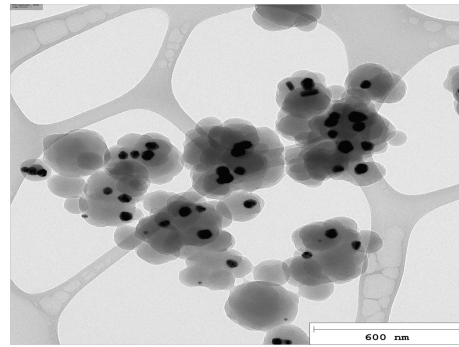


(h) TEM image of experiment L101.

Figure 4.12: FE-SEM and TEM images of TMPTA series of experiments shown in Table 4.7.



(a) FE-SEM image of experiment L93.



(b) TEM image of experiment L93.

Figure 4.13: FE-SEM and TEM images of HDDA series of experiments shown in Table 4.7.

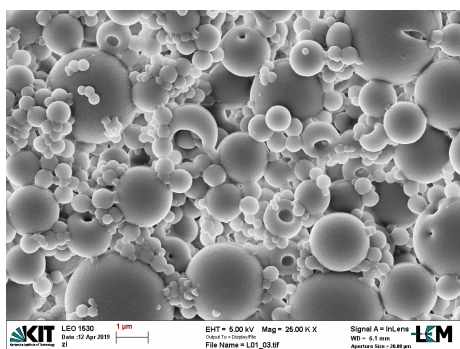
HDDA monomer was also investigated for a non-disrupted structure. However, only a result is shown, since no polymeric material was collected from experiment L94. The amount of photoinitiator here was the 4% of the overall amount of monomer and for this reason, parallel reactions might be boosted. The spray solution turned into a jelly-like substance which forced to stop the experiment before collecting some material.

Instead, experiment L93 showed same results discussed for TMPTA series.

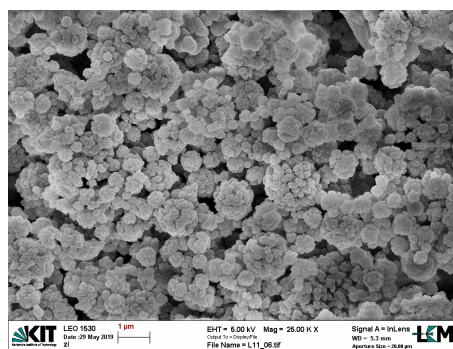
Conclusions

The aerosol photopolymerization technique was used for the production of polymer particles with different size and morfologies. Although microencapsulation was already diffusely realised with liquid-based methods, in the last decade, it has been further investigated combined with advantageous technique. Aerosol photo-induced processes showed several perks for micro and nanoscaled structuring and suitability in an eventual industrial application. Moreover, particles produced can be destined either to the drug delivery in the pharmaceutical field or in numerous physical applications.

Microcapsules were obtained with the combination TMPMP-TMPTA in a solution made up of approximately the same amount of hexadecane, 2-Ethyl-1-hexanol and 2-octanone in acetone or ethanol as a co-solvent with an overall ratio monomers to solvents equal to 33:67. Trifunctionalized or tetrafunctionalized monomers were more suitable for the production of microcapsules because of the capability of creating cross-linked matrix. Also for chain polymerization, the number of functional group of monomers has revealed determinant for obtaining a particular morphology: a mosaic structure was attained with TMPTA, characterized by the presence of nanostructured polymer domains all over the surface. The starting solution kept the same formulation as the one used for microcapsules.



(a) Microcapsules from thiol-ene mechanism.



(b) Structured particles with polymer nanodomains.

Figure 4.14: Comparison between morfologies obtained with different polymerization mechanisms.

Then different composition of the starting spray solution were analysed. With different co-solvents employed, the morfologies of thiol-ene particles produced were significantly changed. On the other hand, no important influences were seen in the acrylic radical polymerization, in which every monomer kept its intrinsic properties. The former mechanism produced capsules also with the combination PETMP-TMPTA in presence of acetone as a high-volatile co-solvent (M/S ratio of 29:71); the latter mechanism produced a disrupted structure when bifunctionalized monomer were employed (Neopentyl and HDDA), the mosaic structure showed beforehand in Figure 4.14b and slight decorated particles with the tetrafunctionalized monomer PETA (renumber of nanodomains visibly reduced).

Facing this results, influence of the M/S ratio was considered for step-growth mechanism, while a M/P ratio was taken into account for the acrylic polymerization. Lowering the M/S ratio, the averaged size of the particles was also lowered to hundreds of nanometers but spherical and non-individual particles were produced. The absence of a high-volatile co-solvent and a high M/S ratio of 50:50, instead, led to the production of big porous sponges. Increasing the M/P ratio with acrylic monomers, spherical nanoparticles with smooth surface were produced thereby highlighting the importance of the role played by porogens in this mechanism. Also the effect of 2-octanone was testes with a result of the reduction of nanodomains number on the particle surface.

For the first time, nanocapsules and nanocaps were produced by adding glycerol to the previous thiol-ene formulations. Both for PETMP-TMPTA and TMPMP-TMPTA, the role of glycerol as a polymer soft-maker was proved. As opposed to what has been said before, experiment with ethanol and 1-propanol as a co-solvent showed the best performances for the process because of the better capability of solubilise the polyol.

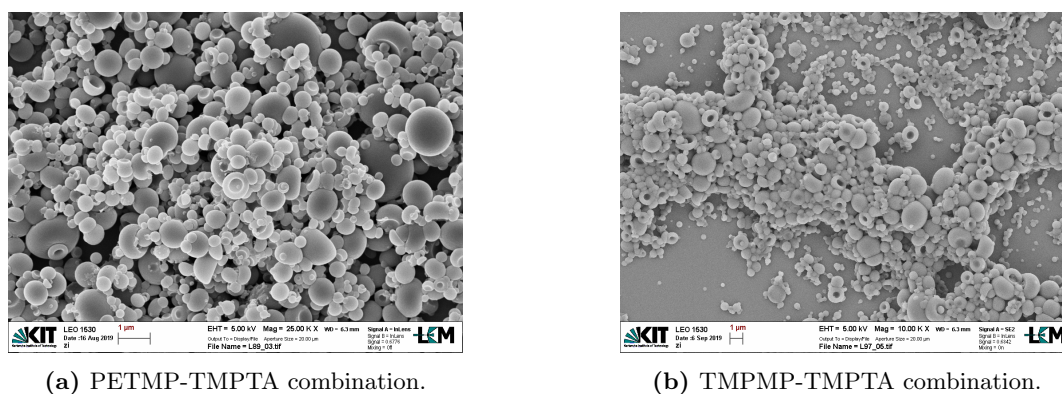


Figure 4.15: Nanocapsules and nanocaps produced by a step-growth mechanism.

Eventually, incorporation *in situ* of silver nanoparticles with a diameter of 50 nm was successfully carried out in mosaic acrylic micro and nanoparticles obtained with TMPTA, whilst same experiment failed for thiol-ene reactions. Agglomerates of silver were found outside the thiol-ene polymeric matrix (Figure 4.16a).

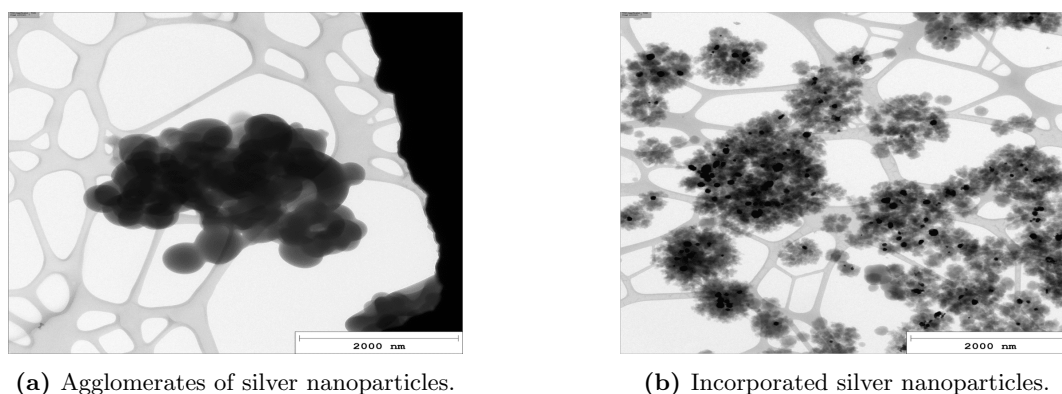


Figure 4.16: Comparison between outcomes obtained with different polymerization mechanisms.

Despite the achievement of this results, a massive amount of experiments could still be conducted to better comprehend the differences between these two polymerization mechanisms. Some tests here conducted showed adaptability problems and no defined causes were found. In the future, new formulations of the spray solution could be sought and investigated together with new apparatuses or new setups, able to handily modify a specific polymeric structure for the application to which will be destined.

List of Figures

1	L'intera strumentazione utilizzata con atomizzatore, reattore e filtro per la raccolta del prodotto.	ii
2	Immagine al FE-SEM di micro-capsule ottenute con TMPMP-TMPTA.	iii
3	Immagini al FE-SEM di particelle di TMPMP-TMPTA ottenute con i diversi co-solventi.	iv
4	Immagini al FE-SEM di particelle TMPMP-TMPTA con rapporto M/S pari a 29:71.	v
5	Immagine al FE-SEM di micro-capsule ottenute con TMPMP-TMPTA.	vi
6	Immagini al FE-SEM di micro-capsule ottenute con meccanismo tiolo-ene.	vii
7	Immagini al FE-SEM di nano-capsule e nano-caps ottenute con meccanismo radicalico tiolo-ene.	viii
8	Immagine al FE-SEM di micro-particelle ottenute con meccanismo radicalico acrilico.	ix
9	Immagini al FE-SEM delle matrici polimeriche ottenute con meccanismo acrilico.	ix
10	Immagini al FE-SEM delle micro-particelle decorate ottenute con meccanismo acrilico.	x
11	Immagini al FE-SEM di micro-particelle ottenute al variare del rapporto M/P.	xi
12	Immagini al FE-SEM di micro-particelle di TMPTA in eventuale presenza di 2-ottanone.	xii
13	Immagini al TEM di particelle ibride ottenute con meccanismo acrilico.	xii
1.1	Categories of microparticles. Figure adapted from (Campos et al., 2013) with modification.	2
1.2	The whole employed setup: on the left the pneumatic atomizer connected to the 4-FEP tube photoreactor (on the right).	3
1.3	Thiol-ene mechanism. Figure adapted from (Cramer and Bowman, 2001) with modification.	4
1.4	Decomposition of Iragacure 907 [®] into two free radicals and the summerized reaction.	5
2.1	ATM 220 by TOPAS.	11
2.2	UGF 2000 by PALAS.	11
2.3	Bottom of the aerosol generator by PALAS.	12
2.4	Quartz tube photoreactor.	12
2.5	The two type of FEP tube reactors.	13
3.1	FE-SEM images of experiments described in Table 3.1.	16
3.2	FE-SEM images of experiments described in Table 3.2.	19
3.3	FE-SEM images of experiments described in Table 3.3.	20
3.4	Keto-enol tautomerism of acetone.	21
3.5	FE-SEM images of experiments described in Table 3.3.	21
3.6	FE-SEM images of experiments described in Table 3.4.	22

3.7	FE-SEM images of experiments described in Table 3.4.	22
3.8	FE-SEM images of experiments described in Table 3.4.	23
3.9	FE-SEM images of experiments described in Table 3.5.	24
3.10	FE-SEM images of experiments described in Table 3.5.	25
3.11	FE-SEM images of experiments described in Table 3.5.	26
3.12	FE-SEM images of experiments described in Table 3.7.	27
3.13	FE-SEM images of experiments described in Table 3.9.	30
3.14	FE-SEM images of experiments described in Table 3.9.	31
3.15	FE-SEM images of experiments described in Table 3.10.	32
3.16	FE-SEM images of experiments described in Table 3.11.	33
3.17	FE-SEM images of experiments described in Table 3.11.	34
3.18	FE-SEM images of experiments described in Table 3.11.	34
3.19	FE-SEM images of experiments described in Table 3.12.	36
3.20	FE-SEM and TEM images of experiments shown in Table 3.13.	37
4.1	FE-SEM images of experiments described in Table 4.1.	40
4.2	FE-SEM images of experiments in Table 4.2 with ethanol as co-solvent.	41
4.3	FE-SEM images of experiments in Table 4.2 with a higher magnification.	42
4.4	FE-SEM images of experiments in Table 4.2 with 1-propanol as co-solvent.	42
4.5	FE-SEM images of experiments in Table 4.2 with acetone as co-solvent.	43
4.6	FE-SEM images of experiments in Table 4.3.	44
4.7	FE-SEM images of experiments in Table 4.3.	45
4.8	FE-SEM images of TMPTA series of experiments shown in Table 4.4.	46
4.9	FE-SEM images of HDDA series of experiments in Table 4.4.	47
4.10	FE-SEM images of TMPTA series of experiments in Table 4.4.	48
4.11	FE-SEM images of experiments in Table 4.6.	49
4.12	FE-SEM and TEM images of TMPTA series of experiments shown in Table 4.7.	51
4.13	FE-SEM and TEM images of HDDA series of experiments shown in Table 4.7.	52
4.14	Comparison between morfologies obtained with different polymerization mechanisms.	53
4.15	Nanocapsules and nanocaps produced by a step-growth mechanism.	54
4.16	Comparison between outcomes obtained with different polymerization mechanisms.	54

List of Tables

3.1	List of experiments with different ene-monomers used.	15
3.2	List of experiments with different thiol-monomers used.	18
3.3	List of experiments with different co-solvents employed.	20
3.4	List of experiments with different co-solvents employed.	22
3.5	List of experiments with different amount of co-solvents.	24
3.6	List of the experiments without co-solvent and different amount of porogens. . .	26
3.7	List of the experiments conducted with the different models of the atomizers. . .	27
3.8	Details of each process configuration.	29
3.9	List of the experiments performed in different photoreactor models.	29
3.10	List of experiment with glycerol and PETMP-TMPTA combination.	31
3.11	List of experiment with glycerol and TMPMP-TMPTA combination.	33
3.12	List of experiments with glycerol and TMPMP-BVE combination.	35
3.13	List of experiments with addition of silver nanoparticles.	36
4.1	List of experiments with acrylic monomers without using a co-solvent.	39
4.2	List of the experiments conducted with acrylic monomers in different co-solvents.	41
4.3	List of experiments with variation of hexadecane.	44
4.4	List of experiments with variation of isooctanol.	45
4.5	List of experiments with same M/P ratio.	47
4.6	List of experiments with variation of 2-octanone.	49
4.7	List of experiments with addition of silver nanoparticles.	50

Acronyms

TMPMP	Thrimethylolpropane Tri(3-mercaptopropionate),
ETTMP 700	Ethoxylated-Thrimethylolpropane Tri(3-mercaptopropionate) with average $M_n \sim 700$
ETTMP 1300	Ethoxylated-Thrimethylolpropane Tri(3-mercaptopropionate) with average $M_n \sim 1300$
GDMP	Glycol Di(3-mercaptopropionate)
GDMA	Glycol Dimercaptoacetate
PETMP	Pentaerythritol Tetra(3-mercaptopropionate)
TEMPIC	Tris[2-(3-mercaptopropionyloxy)ethyl] isocyanurate
TMPTA	Trimethylolpropane triacrylate
Diallyl	Diallyl Adipate
Neopentyl	Neopentyl glycol diacrylate
Triallyl-T	1,3,5-Triallyl-1,3,5-triazine-2,4,6(1H,3H,5H)-trione
DVE	Tri(ethylene glycol) divinyl ether
TMPe7TA	Trimethylolpropane ethoxylate triacrylate
DVA	Divinyl Adipate
TVC	1,2,4-Trivinyl cyclohexane
HDDA	1,6-hexanediol diacrylate
PETA	Pentaerythritol tetraacrylate
BVE	1,4-Butanediol divinyl ether
HD	Hexadecane
2-OCT	2-Octanone,
ISO	2-Ethyl-1-hexanol
EtOH	Ethanol
PrOH	1-Propanol
MEHQ	4-Methoxyphenol

Bibliography

- Akgün E., Hubbuch J. and Wörner M. (2014). Perspectives of aerosol-photopolymerization: organic-inorganic hybrid nanoparticles. *Colloid and Polymer Science* **292**, pp. 1241–1247. [DOI:10.1007/s00396-014-3175-2].
- Akgün, E., Hubbuch J., and Wörner M. (2013). Perspectives of aerosol-photopolymerization: Nanoscale polymer particles. *Chem. Eng. Sci.* **101**, pp. 248–252. [DOI:10.1016/j.ces.2013.06.010].
- Anton, N., Benoit J.P., and Saulnier P. (2008). Design and production of nanoparticles formulated from nano-emulsion templates—a review. *J. of controlled release* **128**, pp. 185–199. [DOI:10.1016/j.jconrel.2008.02.007].
- Bazzano, M., Latorre D., Pisano R., and Sangermano M. (2017). Nano-structured polymeric microparticles produced via cationic aerosol photopolymerization. *Journal of Photochemistry and Photobiology A: Chemistry* **346**, pp. 364–371. [DOI:10.1016/j.jphotochem.2017.06.009].
- Benita, S. (2005). *Microencapsulation: Methods and Industrial Applications*. Ed. by Taylor and Francis Group. Second edition. Vol. 158.
- Biskos, G., Vons V., Yurteri C., and Schmidt-Ott A. (2008). Generation and Sizing of Particles for Aerosol-Based Nanotechnology. *KONA Powder and Particle Journal* **26**, pp. 13–35. [DOI:10.14356/kona.26.2008006].
- Boguslavskii, Y.Y. and Eknadiosyants O.K. (1969). Physical mechanism of the acoustic atomization of a liquid. *Soviet Phys. Acoust.* **15**, pp. 14–21.
- Bungenberg, H.G. (1932). Die Koazervation und ihre Bedeutung für die Biologie. *Protoplasma* **15**.
- Campos, E., Branquinho J., Carreira A.S. and Carvalho A., Coimbra P., Ferreira P., and Gil M.H. (2013). Designing polymeric microparticles for biomedical and industrial applications. *European Polymer Journal* **49**, pp. 2005–2021. [DOI:10.1016/j.eurpolymj.2013.04.033].
- Cramer, N. and Bowman C. (2001). Kinetics of Thiol-Ene and Thiol-Acrylate Photopolymerizations with Real-Time Fourier Transform Infrared. *Journal of Polymer Science* **39**, pp. 3311–3319.
- Cruz, L., Soares L.U., Costa T.D., Mezzalira G., da Silveira N.P., Guterres S.S., and Pohlmann A.R. (2006). Diffusion and mathematical modeling of release profiles from nanocarriers. *International Journal of Pharmaceutics* **313**, pp. 198–205. [DOI:10.1016/j.ijpharm.2006.01.035].
- Esen, C. and Schweiger G. (1996). Preparation of monodisperse polymer particles by photopolymerization. *Journal of colloid and interface science* **179**, pp. 276–280. [DOI:10.1006/jcis.1996.0214].
- Esen, C., Kaiser T., and Schweiger G. (1996). Photopolymerization reactions in aerosols: a simple method to the synthesis of monodisperse microspheres. *J. Aerosol Sci.* **27**, pp. 371–372.
- Esen, C., Kaiser T., Borchers M.A., and Schweiger G. (1997). Synthesis of spherical microcapsules by photopolymerization in aerosols. *Colloid and Polymer Science* **275**, pp. 131–137. [DOI:10.1007/s003960050062].
- Esfandiari, P., Ligon S., Lagref J., Frantz R., Cherkaoui Z., and Liska R. (2013). Efficient Stabilization of Thiol-ene Formulations in Radical Photopolymerization. *Journal of Polymer Science* **51**, pp. 4261–4266. [DOI:10.1002/pola.26848].
- Fattal, E. and Vauthier C. (Jan. 2002). Nanoparticles as drug delivery systems. *Encyclopedia of Pharmaceutical Technology*, pp. 1864–1882.

- Furtado, V.C., Legrand P., Gulik A., Bourdon O., Gref R., Labarre D., and Barratt G. (2001). Relationship between complement activation, cellular uptake and surface physicochemical aspects of novel PEG-modified nanocapsules. *Biomaterials* **22**, pp. 2967–2979. [DOI:10.1016/s0142-9612(01)00043-6].
- Guinebretière, S., Briancon S., Fessi H., Teodorescu V.S., and Blanchin M.G. (2002). Nanocapsules of biodegradable polymers: preparation and characterization by direct high resolution electron microscopy. *Material Science and Engineering* **21** (1-2), pp. 137–142. [DOI:10.1016/S0928-4931(02)00073-5].
- Holliday, W.M., Berdrick M., Bell S.A., and Kiritsis G.C. (1970). “Sustained relief analgesic compositions”. US3524910A.
- Liu, W. (2006). Nanoparticles and their biological and environmental applications. *Journal of Bioscience and Bioengineering* **102**, pp. 1–7. [DOI:10.1263/jbb.102.1].
- Oster G., Yang N.L. (1968). Photopolymerization of vinyl monomers. *Chem. Rev.* **68** (2), pp. 125–151. [DOI:10.1021/cr60252a001].
- Peiffer, R.W. (1997). Photopolymerization of vinyl monomers. *ACS Symposium Series* **673**, pp. 1–14. [DOI:10.1021/bk-1997-0673.ch001].
- Raula, J., Eerikäinen H., and Kauppinen E.I. (2004). Influence of the solvent composition on the aerosol synthesis of pharmaceutical polymer nanoparticles. *International Journal of Pharmaceutics* **284**, pp. 13–21. [DOI:10.1016/j.ijpharm.2004.07.003].
- Reis, C.P., Neufeld R.J., Ribeiro A.J., and Veiga F. (2006). Nanoencapsulation I. Methods for preparation of drug-loaded polymeric nanoparticles. *Nanomedicine* **2** (1), pp. 8–21. [DOI:10.1016/j.nano.2005.12.003].
- Shaban, M., Ramazani S.A., Ahadian M.M., Tamsilian Y., and Weber A.P. (2016). Nanoencapsulation I. Methods for preparation of drug-loaded polymeric nanoparticles. *European Polymer Journal* **83**, pp. 323–336. [DOI:10.1016/j.eurpolymj.2016.08.022].

Acknowledgements

First of all, I would like to warmly thank prof. Michael Wörner for have been constantly present during my stay in Karlsruhe. He showed himself very helpful in every situation, from my needs in ordinary life to every problem I faced in the working context. He has been clear and patient in every situation.

Of course I want to acknowledge also prof. Marco Sangermano for having given me this opportunity to work for such important project which has improved my personal skills and my capability of settling in a different country far from my home.

A special thank goes also to all the people that supported me for this long experience. In the first place my family for having encouraged and helped me for the whole stay in Turin. Then, I would like to mention all my friends which I spent most of the time with, especially who hosted me in difficult times.

I dedicate the achievement of this goal to my mother, who put a lot of effort to sustain me and now, if only she could, she would certainly wanted to see me so realised as I am in this moment.